JOURNAL OF GEOPHYSICAL RESEARCH, VOL. 104, NO. B4, PAGES 7443–7462, APRIL 10, 1999

Deep structure of the ocean-continent transition in the southern Iberia Abyssal Plain from seismic refraction profiles: Ocean Drilling Program (Legs 149 and 173) transect

Deping Chian[1] and Keith E. Louden

Department of Oceanography, Dalhousie University, Halifax, Nova Scotia, Canada

Tim A. Minshull

Bullard Laboratories, Department of Earth Sciences, University of Cambridge, Cambridge, England

Robert B. Whitmarsh

Challenger Division, Southampton Oceanography Centre, Southampton, England

Abstract. We present a wide-angle seismic refraction study of an 80x40 km region of the southern Iberia Abyssal Plain, south of Galicia Bank. An intersecting grid of two E-W and four N-S wide-angle reflection/refraction profiles is used to define variations of the basement velocity structure within this unusually wide ocean-continent transition (OCT). These structures can be systematically linked to variations in acoustic basement morphology and to results from Ocean Drilling Program (ODP) boreholes. Lateral changes in the velocity structure of the basement occur abruptly over distances of ~20 km where complex variations may be found. Thinned upper continental crust, 2-5 km thick with velocities of 5.0-6.6 km/s, is limited to a series of N-S fault blocks immediately south of Galicia Bank. This crust is underlain by a high-velocity layer (7.3-7.9 km/s) of weakly serpentinized (i.e., 0-25%) peridotite, which exists throughout the eastern part of the survey area. Basement within the OCT appears to consist dominantly of a broad region of exposed upper mantle that has been serpentinized heterogeneously both vertically and horizontally. In the southeast sector of our survey where basement topography deepens and becomes subdued, continental fault blocks are absent; instead, basement contains an upper layer of more pervasively serpentinized (i.e., 25-45%) peridotite that is ~2 km thick. This layer is characterized by low velocity at the top of basement (4.2 km/s) that increases rapidly with depth, and it probably corresponds to a seismically unreflective layer, previously identified in reflection profiles to the south of our survey. In the western section of our survey, beneath a series of elevated basement ridges, velocities are reduced within both the upper basement layer (3.5-6.0 km/s) and lower layer (6.4-7.5 km/s). These changes suggest that both upper and lower layers have become more highly serpentinized (with values of 60-100% in the upper layer and 25-45% in the lower layer) probably during the last stages of rifting and immediately before formation of oceanic crust. A normal or slow spreading oceanic crustal structure is not found within the survey region. Thus it appears that the onset of seafloor spreading occurs in the region west of the peridotite ridge sampled at ODP Site 897 and east of the J magnetic anomaly.

1. Introduction

Delineating the nature of crustal variations across passive continental margins is fundamental to our understanding of how the uppermost lithosphere deforms under extension. This information is best obtained from joint analysis of coincident deep multichannel seismic reflection and wide-angle reflection/refraction profiles, across margins where the extensional fabric within the crust has not been significantly modified or obscured by large-scale synrift volcanism. Results of previous studies primarily in the North Atlantic have shown a range of extensional styles. For instance, reflection and wide-angle reflection/refraction profiles across Goban Spur (GS in Figure 1) [*Peddy et al.*, 1989; *Horsefield et al.*, 1994] define a consistent pattern of seawardly progressive, homogeneous thinning of the continental crust over a distance of at least 100 km. These observations are compatible with models of pure shear extension [*McKenzie*, 1978] and are consistent with observed variations in heat flow [*Louden et*

[1]Now at Geological Survey of Canada (Atlantic), Dartmouth, Nova Scotia, Canada.

Paper number 1999JB900004.
0148-0227/99/1999JB900004$09.00

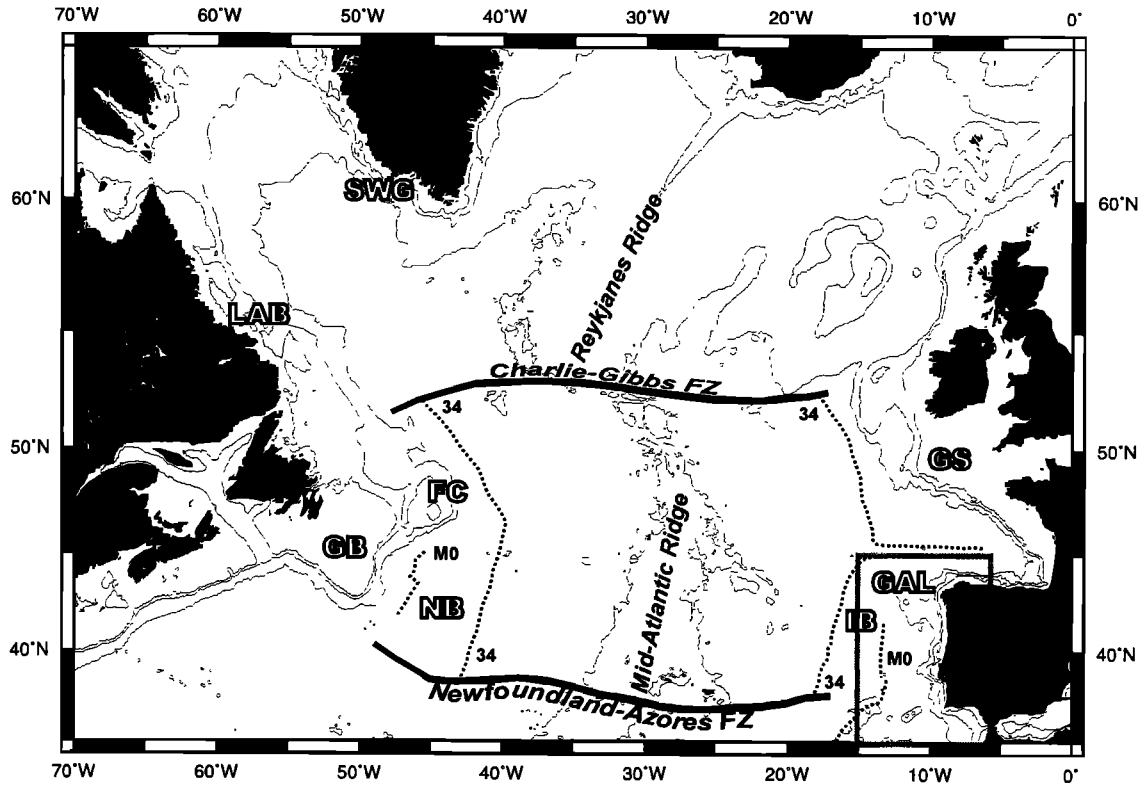

Figure 1. Map of the North Atlantic showing key areas discussed in the text. M0 and 34 are magnetic anomalies from *Klitgord and Schouten* [1986]. Small rectangle shows area of Figure 2. IB, Iberia Abyssal Plain; GAL, Galicia Bank; GS, Goban Spur; GB, Grand Banks of Newfoundland; FC, Flemish Cap; NB, Newfoundland Basin; LAB, Labrador margin; SWG, Southwest Greenland margin; FZ, fracture zone.

al., 1991]. In contrast, profiles across Galicia Bank (GAL in Figure 1) [*Mauffret and Montadert*, 1987; *Whitmarsh et al.*, 1996] indicate a more complex style of extension, which has been explained by models with various combinations of pure and simple shear [e.g., *Winterer et al.*, 1988; *Boillot et al.*, 1989; *Sibuet et al.*, 1995]. At both margins, however, a relatively abrupt transition occurs between the extended continental crust and the seaward formation of oceanic crust. At Goban Spur, this occurs just west of a volcanic sill; while off Galicia Bank, the landward edge of oceanic crust is marked by a well-defined peridotite ridge (i.e., an elongated basement high composed of hydrated upper mantle rocks [*Boillot et al.*, 1980; *Sibuet et al.*, 1995]).

On other margins, a much wider transition region exists between extended continental crust and typical oceanic crust. This zone has a rather uncertain crustal affinity, though in general it is thought to have formed during prolonged periods of extension when little or no melt is generated from the mantle [*Bown and White*, 1995]. Recent profiles across the Labrador (LAB in Figure 1) and SW Greenland (SWG in Figure 1) conjugate margins [*Chian and Louden*, 1994; *Keen et al.*, 1994; *Chian et al.*, 1995a, b] show a transition zone on each margin, situated between rifted and thinned continental crust and typical oceanic crust. Each zone is characterized by unusually low basement velocities (~4.5 km/s) and high (7.2-7.6 km/s) underlying velocities at subbasement depths of 2-3 km. The landward boundary of each zone is marked by rotated fault blocks, and the seaward boundary is marked by an abrupt shallowing of the basement. Reflections from the Moho boundary are absent within the transition zone. Similar velocity structures have also been observed across the Newfoundland continental margins (FC and GB in Figure 1) [*Reid and Keen*, 1990; *Reid*, 1994].

A similar ocean-continent transition (OCT) has been extensively investigated in the southern Iberia Abyssal Plain (Figure 2 and Plate 1) [*Whitmarsh et al.*, 1990, 1993; *Whitmarsh and Miles*, 1995], particularly along a recently completed E-W transect of Ocean Drilling Program (ODP) boreholes [*Sawyer et al.*, 1994; *ODP Leg 173 Shipboard Scientific Party*, 1998; *Whitmarsh et al.*, 1998]. However, until recently, the origin of the basement within the transition region remained uncertain, with several suggested possibilities [*Whitmarsh and Sawyer*, 1996]: (1) thinned continental crust intruded by melt from the mantle; (2) thin and tectonized oceanic crust produced by ultraslow seafloor spreading; and (3) serpentinized upper mantle. Most recently, preliminary results of wide-angle seismic data [*Discovery 215 Working Group*, 1998] suggest that this transition zone is associated with an extensive region of anomalously high velocity at a depth of 2-5 km below the topmost basement and has a velocity structure which is significantly different from oceanic crust. It is clear as well, however, that the transition region exhibits significant variations across, as well as along, strike of the margin.

In this paper we will present detailed results from models of the wide-angle seismic data in the region of the ODP transect (Plate 1). While previous studies across ocean-continent transitions have been limited to the analysis of single

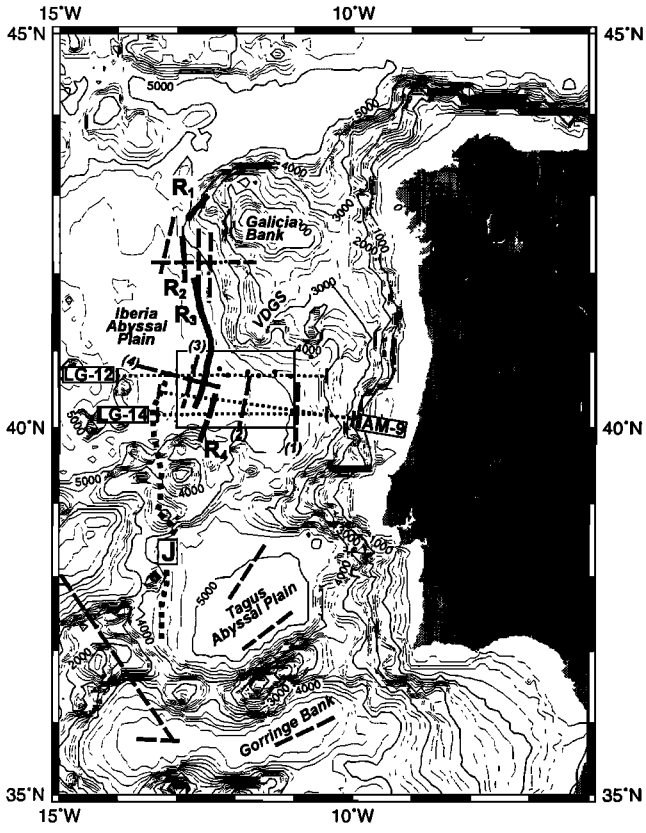

Figure 2. Bathymetric chart of the West Iberia margin. Thin contours show bathymetry every 200 m; bold contours show bathymetry every 1000 m. Sites drilled by ODP Legs 173 and 149 are marked by solid circles. Dashed lines are refraction profiles of *Whitmarsh et al.* [1990] in the Iberia Abyssal Plain (1-4), of *Pinheiro et al.* [1992] in the Tagus Abyssal Plain, and of *Whitmarsh et al.* [1996] west of Galicia Bank. Thin dotted lines (LG-12, LG-14, and IAM-9) are selected multichannel seismic (MCS) reflection lines in the study area. R_1, R_2, R_3, and R_4 are segments of peridotite ridge [after *Beslier et al.*, 1993; *Discovery 215 Working Group*, 1998]. VDGS, Vasco da Gama Seamount. Rectangle shows area of Plate 1.

transects, in this case we are able to utilize an intersecting grid of two E-W and four N-S profiles to investigate three-dimensional (3-D) characteristics of the transition region.

2. Southern Iberia Abyssal Plain

The study area lies within the southern Iberia Abyssal Plain, west of the central Iberia peninsula, south of Galicia Bank, and north of the Tagus Abyssal Plain (Figure 2 and Plate 1). This margin is nonvolcanic and formed as a result of several stages of Mesozoic rifting between the Grand Banks and Iberia [e.g., *Pinheiro et al.*, 1996]. Initial continental stretching started in the Late Triassic and was followed by three main rifting phases up to the Early Cretaceous. The first unequivocal seafloor spreading anomaly in this region is the J anomaly (Figure 2), which lies between magnetic chrons M0 and M2 [e.g., *Tucholke and Ludwig*, 1982]. However, *Whitmarsh and Miles* [1995] and *Whitmarsh et al.* [1996] matched additional anomalies to the reversal timescale up to 20 km landward of the J anomaly, suggesting that seafloor spreading began west of the peridotite ridges (Figure 2) during M3 time. Plate reconstructions to Chron M0 [*Srivastava and Verhoef*, 1992] join Galicia Bank to Flemish Cap (Figure 1), but leave a deep water ocean-continent transition (OCT) zone up to 180 km wide between the J anomaly and the base of the Iberia continental rise (Figure 2).

ODP Legs 103, 149, and recently 173 have sampled a number of sites within this deep water part of the OCT off West Iberia (Plate 1 and Figure 3). Sites 897, 899, 1067, and 1070 sampled serpentinized peridotite [*Sawyer et al.*, 1994; *ODP Leg 173 Shipboard Scientific Party*, 1998; *Whitmarsh et al.*, 1998], with Site 897 likely representing a southward continuation of the peridotite ridge sampled off western Galicia Bank (for location see R1-R4 in Figure 2) [*Boillot and Winterer*, 1988; *Beslier et al.*, 1993]. Site 900 sampled a mid-ocean ridge basalt (MORB)-like gabbro that was tectonically exhumed above the 200-250°C isotherm at 136.4±0.3 Ma during the final extension of the continental crust and before the onset of seafloor spreading [*Féraud et al.*, 1996]. This site is located over a probable fault block, imaged on multichannel seismic (MCS) reflection profile LG-12, just west of a strong midcrustal H reflector that may be offset toward the surface (Figure 3) [*Beslier*, 1996; *Krawczyk et al.*, 1996; *Dean et al.*, 1998]. The H reflector is well imaged on profile LG-12 between Sites 900 and 1065, and another horizontal reflector occurs in the vicinity of Site 1069 (Figure 3). These reflectors have an appearance similar to the S reflector beneath the Galicia Bank, which has been given a number of interpretations: (1) a lithospheric detachment fault in a simple shear model [*Winterer et al.*, 1988]; (2) an intracrustal detachment fault in a composite pure and simple shear model [*Sibuet*, 1992]; (3) a boundary between crust and serpentinized peridotite [*Boillot et al.*, 1989]; and (4) a crust/serpentinite boundary seaward and an intracrustal fault landward [*Whitmarsh et al.*, 1996]. Sites 901, 1065, and 1069 sampled Jurassic prerift sediment not younger than Tithonian (~150 Ma), suggesting a link between the occurrence of the H reflector and the presence of rifted continental crust. The existence of continental crust is also consistent with an extensive region east of Site 900 where heat flow is unusually high [*Louden et al.*, 1997].

West of ODP Site 1069 the reflectivity along LG-12 changes (Figure 3). No horizontal intrabasement reflectors are present beneath the elevated basement sampled by ODP Sites 897, 898, and 1070. In addition, only 50 km south of LG-12, the H reflector does not exist at all. Instead, within the ~130-km wide OCT along profile IAM-9 (Plate 1), a thin (1.0-2.5 km thick) and acoustically unreflective layer is observed overlying a more reflective subbasement layer [*Pickup et al.*, 1996]. *Pickup et al.* [1996] interpret this structure to be a result of serpentinization of upper mantle peridotites, with the unreflective upper basement layer representing a zone of more extensive (but downward decreasing) serpentinization. North-south changes are also observed in the basement morphology and magnetic anomalies [*Whitmarsh and Miles*, 1995; *Discovery 215 Working Group*, 1998] which, when viewed in conjunction with ODP sampling and MCS profiles, indicate a rather complex three-dimensional structure in the study area.

Four seismic refraction lines have been acquired previously in the southern Iberia Abyssal Plain (Figure 2 and Plate 1) [*Whitmarsh et al.*, 1990] to study the velocity structure in the deep water part of the margin. These data indicated the

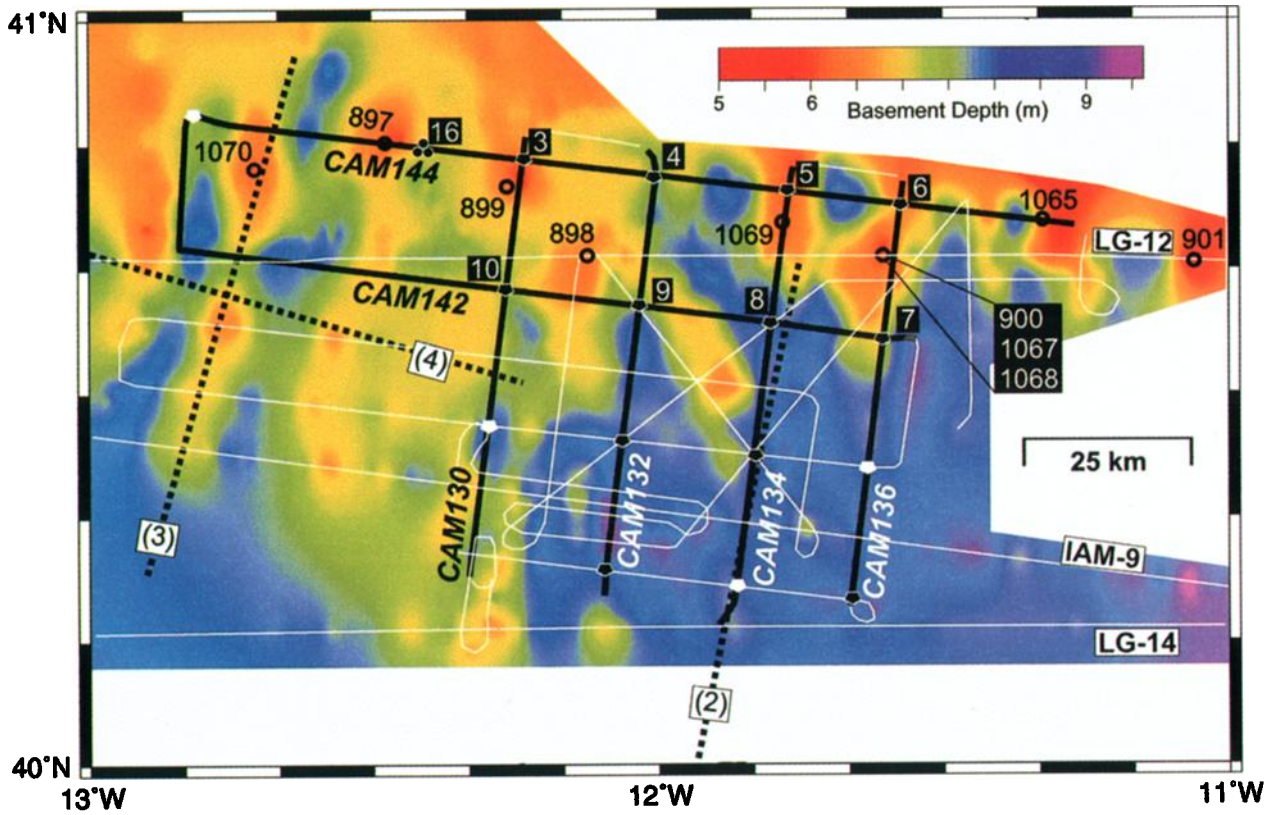

Plate 1. Detailed map of six seismic refraction lines (thick solid lines) for this study. The background image is a mapping of depth to basement (in km) [after *Discovery 215 Working Group*, 1998]. The eight OBS are labeled as 3-10 (successful OBS marked by solid polygons; malfunctioned OBS by open polygons) and a single sonobuoy is labeled 16. Thick dotted lines labeled (2), (3), and (4) are previous refraction lines of *Whitmarsh et al.* [1990]. LG-12, LG-14, and IAM-9 are other deep MCS reflection lines. All other white lines are MCS seismic lines shot during cruise *Discovery* 215 but not included in this paper.

presence of high velocities (>7.2 km/s) at rather shallow depths, overlain by a thin basement layer (1.0-2.5-km thick) with low velocity (4.5-6.5 km/s). While it is possible that the velocities in excess of 7.2 km/s on these profiles represent either serpentinized peridotite [e.g., *Whitmarsh et al.*, 1993; *Chian et al.*, 1995a, b] or a lower oceanic crustal layer of mafic gabbro [e.g., *Whitmarsh et al.*, 1990, 1993; *Srivastava and Roest*, 1995], the limited data density that existed in the Iberia Abyssal Plain prevented more definitive interpretations as to where the continental crust ends and oceanic crust starts. In this paper, we will present a much more detailed analysis of new seismic refraction data in this region that further details the nature of this transition zone.

3. Data Acquisition and Processing

A number of intersecting MCS profiles were shot in a 130x60 km area of the OCT, with the major lines spaced ~20 km apart in both the N-S and E-W directions (Plate 1). The source was a tuned array of 12 air guns with a total capacity of 104.1 L (6346 inch^3) deployed at 20 m water depth and fired every 40 or 50 s for a shot interval of ~100 m. Out of 16 digital ocean bottom seismometers (OBS) that were deployed at the intersections of the eight major N-S and E-W reflection lines, 11 concurrently recorded a selected number of airgun shots depending on the limit of OBS recording time. These OBS were of various types from Dalhousie University, Cambridge University, and Southampton Oceanography Centre (formerly from IOSPL Wormley), as described in Table 1. Five of the OBS in the southern region of the grid malfunctioned. A few sonobuoys (S/B) were also deployed, with rather limited data quality, only one of which (16 in Plate 1) is modeled in this paper.

We model the wide-angle data from the two-dimensional OBS grid recording shots along two E-W refraction lines (CAM144 and CAM142 perpendicular to the J anomaly), and along four N-S refraction lines (CAM130, 132, 134, and 136) in the northern part of this survey (Plate 1). These lines crossed or were close to ODP Sites 897-901, 1065, and 1067-1070 (Plate 1). Migrated reflection data along these lines, which provide clear images over the sediment structures and most of the basement surfaces, were used for the construction of initial velocity models for wide-angle modeling. In one case, a strong intrabasement reflection is observed ("H_1" in Figure 4b), similar to the H reflector imaged farther south along the LG-12 MCS line [*Krawczyk et al.*, 1996]. A few other intrabasement reflectors also exist along these MCS lines, but with much less clarity than the H_1 reflector. Details of the MCS reflection data will be presented in a separate paper.

Differential Global Positioning System (GPS) was used to determine the shot positions, with an error of <10 m. The locations of OBS on the seafloor were corrected using water wave arrivals to an accuracy of ~100 m. All OBS data were corrected for OBS clock drift and shot delay. Further

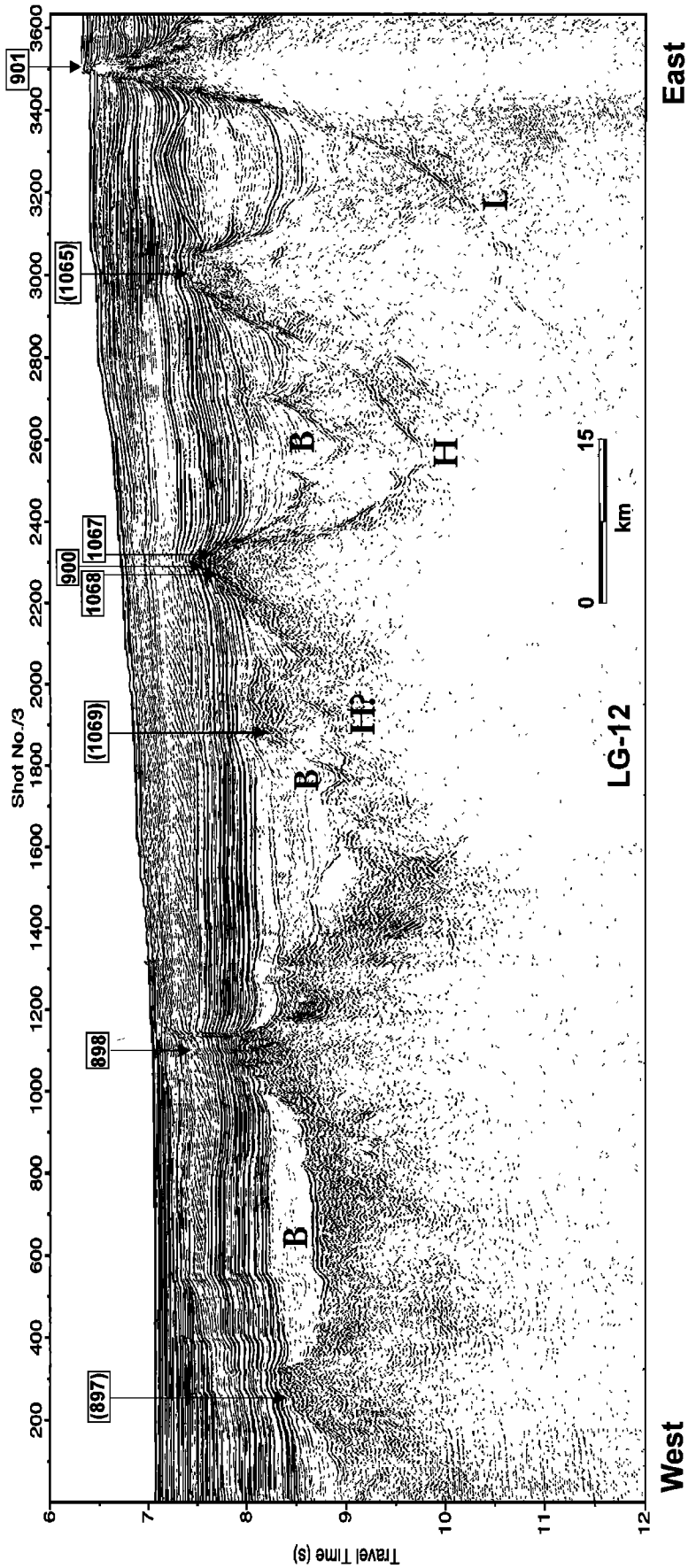

Figure 3. Part of a time-migrated multichannel seismic reflection profile (LG-12) [*Beslier*, 1996] in the study area showing topographical features of basement (B), intrabasement reflectors (H and L) after *Krawczyk et al.* [1996], and locations of ODP sites (projected positions indicated by parentheses) of Legs 149 [*Sawyer et al.*, 1994] and 173 [*ODP Leg 173 Shipboard Scientific Party*, 1998].

Table 1. OBS/Sonobuoy Locations

Sensor Position	Latitude, °N	Longitude, °W	Sensor Depth, m	Recording Package	Sensor Type	Sampling Rate, Hz
3	40.8151	12.2373	5212	M	H	256
4	40.7938	12.0052	5100	D	H+G[3]	173
5	40.7715	11.7741	4986	B	H	64
6	40.7517	11.5769	4908	D	H+G[3]	173
7A	40.5738	11.6043	5093	B	H	128
7B	40.5727	11.6078	5094	W	H+G[1]	100
8	40.5911	11.8013	5144	M	H	256
9	40.6211	12.0316	5191	D	H+G[3]	173
10	40.6430	12.2644	5231	M	H	256
16	40.8308	12.4072	90	W	Sonobuoy	100

M, Cambridge mini-DOBS; B, Cambridge DOBS; W, Wormley DOBS; D, Dalhousie DOBS; H, hydrophone only; H+G[1], hydrophone and one-component geophone; H+G[3], hydrophone and three-component geophone; OBS 7A only recorded shots on CAM136; OBS 7B only recorded shots on CAM142.

processing includes band-pass filtering of 3-10 Hz, clipping of high amplitudes, gain increasing linearly with horizontal range, and coherency mixing [*Chian and Louden*, 1992] of seven adjacent shots scanned at velocities between 2.5 and 8.5 km/s. Owing to the large number of OBS profiles to be presented, the wide-angle phases are picked from the hydrophone data and displayed as error bars, representing the estimated travel time uncertainty, overlain with computed travel time curves. The travel time uncertainty is set such that a clear phase has an uncertainty of one fourth of its dominant wavelength. For example, P_2 of OBS 3 in Figure 5a, and the water waves of all OBS profiles, are very clearly observed and therefore their error bars span 40 ms (assuming a central frequency of 6 Hz). Deeper phases have larger uncertainties. For example, the P_3 phase observed on OBS 8 at 40 km distance in Figure 5c is associated with an error bar of 100 ms. For each seismic phase, one pick with associated error bar represents ~3-6 traces. Weaker arrivals generally result in fewer picks identified from the time sections. For a complete display of seismic record sections for all OBS, refer to the electronic supplement[1].

4. Two-Dimensional Modeling

We use the 2-D ray-tracing algorithm of *Zelt and Smith* [1992] for modeling the wide-angle data. Two-way travel times of sediment reflectors from coincident MCS reflection data (e.g., Figure 4b) are converted to depth using interval velocities obtained from the wide-angle data, thus establishing the model geometry above the basement. Each model is constructed with 10 individual boundaries (forming nine layers), each of which contains up to 63 boundary nodes. The velocities within each layer are specified by up to 19 velocity nodes for the top and bottom boundaries of the layer.

The three-dimensional grid design of the seismic lines shown in Plate 1 is useful in defining the structures within the OCT region, where greater variations in basement topography occur from west to east than from north to south. This allows better control on basement velocity along the four N-S lines (CAM130, 132, 134, and 136). Velocity models obtained from these N-S lines provide important controls on the modeling of the more complex E-W lines.

We identify individual wide-angle seismic phases using the following convention (examples of which are shown in Figure 4a): (1) P_{1a} to P_{1d} represent refractions from four sediment layers, with P_{1c} and P_{1d} easily distinguishable on many wide-angle sections; (2) P_2 and P_3 are refractions from upper and lower basement layers; and (3) P_mP is the reflection from the base of the lower basement layer, and mantle refractions and intramantle reflections are labeled as P_n and $P_{m2}P$, respectively.

4.1. Sediment Layers

The MCS reflection data provide clear images of the sediment layers and most of the basement surface (e.g., Figure 4b). Based on these profiles, we defined four layers for the <4-km-thick sediment. Sediment layer 1a and layer 1b are <1 km thick in total, with velocities of 1.52-2.2 km/s and 2.2-2.3 km/s, respectively, based on measurements on core samples from ODP Sites 899 and *Sawyer et al.* [1994]. Sediment layer 1c is characterized in the reflection data by strong reflectivity throughout its entire (<1.5 km) thickness. Wide-angle refractions from this layer are observed on nearly all N-S profiles (Figure 5), suggesting a velocity of 2.8-3.1 km/s on the eastern lines and 2.5-2.7 km/s on the western lines (Figure 6). These velocities are adjusted by ~0.1 km/s to model P_{1c} at OBS 3 and OBS 5 on CAM144 (Figure 7) and OBS 7-10 on CAM142 (Figure 8), mostly due to variable thickness of this layer caused by basement relief (Figures 6 and 9).

The deepest sediment layer 1d is seen in the reflection profiles as a group of reflective events with a pattern different from overlying sediments and underlying basement (e.g., Figure 4b). Refractions (P_{1d}) from this layer are observed by OBS 8 on CAM134 (Figure 5c) and CAM142 (Figure 8) and OBS 9 on CAM132 (Figure 5b). Travel time modeling yields a velocity gradient from 3.9 to 4.3 km/s. On other OBS profiles, P_{1d} is not well-defined, mostly due to the existence of rough basement topography.

[1]Supporting figures are available on diskette or via Anonymous FTP from kosmos.agu.org, directory APEND (Username - anonymous, Password = guest). Diskette may be ordered from American Geophysical Union, 2000 Florida Avenue, N.W., Washington, DC 20009 or by phone at 800-966-2481; $15.00. Payment must accompany order.

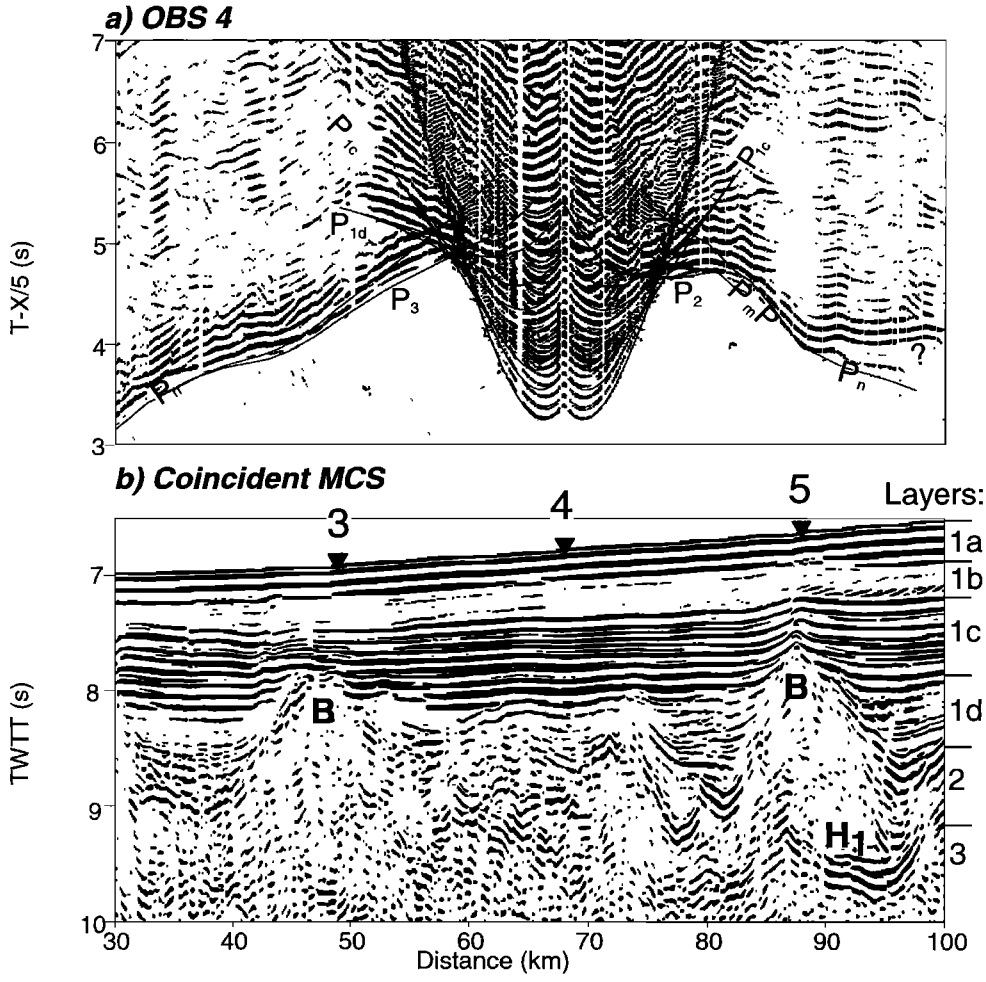

Figure 4. (a) An example of wide-angle OBS data, showing phases from sediment (P_{1c} and P_{1d}), upper basement (P_2), lower basement (P_3), Moho (P_mP), and upper mantle (P_n). Computed travel time curves from the velocity model in Figure 9a are overlain. Phase above the question mark (?) is an unknown phase, possibly caused by out of plane reflectors. (b) A segment from multichannel seismic (MCS) reflection profile CAM144 coincident with Figure 4a. B, basement; H_1, a reflector similar to the H reflector of *Krawczyk et al.* [1996]. Layers 1a-d are four sediment layers used for the velocity modeling. Layers 2 and 3 are upper and lower basement layers, as defined in the text.

4.2. Upper Basement Layer

A prominent feature of the basement topography is the presence of large (up to 3 km high) basement ridges elongated in the N-S direction (e.g., Plate 1). Because the relief is of longer wavelength on N-S lines, we constrain the velocity structure of the upper basement primarily from OBS data on the N-S lines. These results are then applied to the modeling of upper basement along the E-W lines.

4.2.1. N-S lines. The four N-S refraction lines (CAM130, CAM132, CAM134, CAM136) are numbered sequentially from west to east and situated ~20 km from each other (Plate 1). A slight landward increase in velocity is observed near the basement surface from 3.4±0.2 km/s at the shallowest basement ridge on CAM130 to <4.8 km/s on CAM134 and CAM136 (Figure 6). A large vertical gradient of <1.3 s^{-1} exists in this layer, resulting in clear refraction arrivals P_2 wherever basement relief permits (Figure 5). P_2 is observed by most of the OBS along the N-S lines in three different forms:

1. P_2 is best observed as a first arrival by OBS 3 on CAM130 (Figure 5a), where it appears as a steep (very low apparent velocity) phase due to the Site 899 basement high and strong vertical velocity gradient from 3.4 to 6.0 km/s (Figure 6a). This velocity range is consistent with laboratory measurements on core samples from the top of acoustic basement at this site, which have a scattered velocity distribution between 3.4 and 5.1 km/s [*Sawyer et al.*, 1994].

2. As a second arrival, P_2 arrives much later than and is therefore well separated from P_3. An example is OBS 10 of CAM130 (Figure 5a; and also in Figure 11), where the basement velocity (4.0-5.2 km/s) is quite low, forming a large velocity contrast with the underlying layer (Figure 6a).

3. When the velocity of the deepest sediment layer 1d approaches the basement velocity, arrivals from P_{1d} and P_2 merge. All profiles but CAM130 record this case (e.g., OBS 9 on Figure 5b and OBS 8 on Figure 5c).

Complications exist in the velocity structures of the upper basement along CAM134 and CAM136. In particular, north of

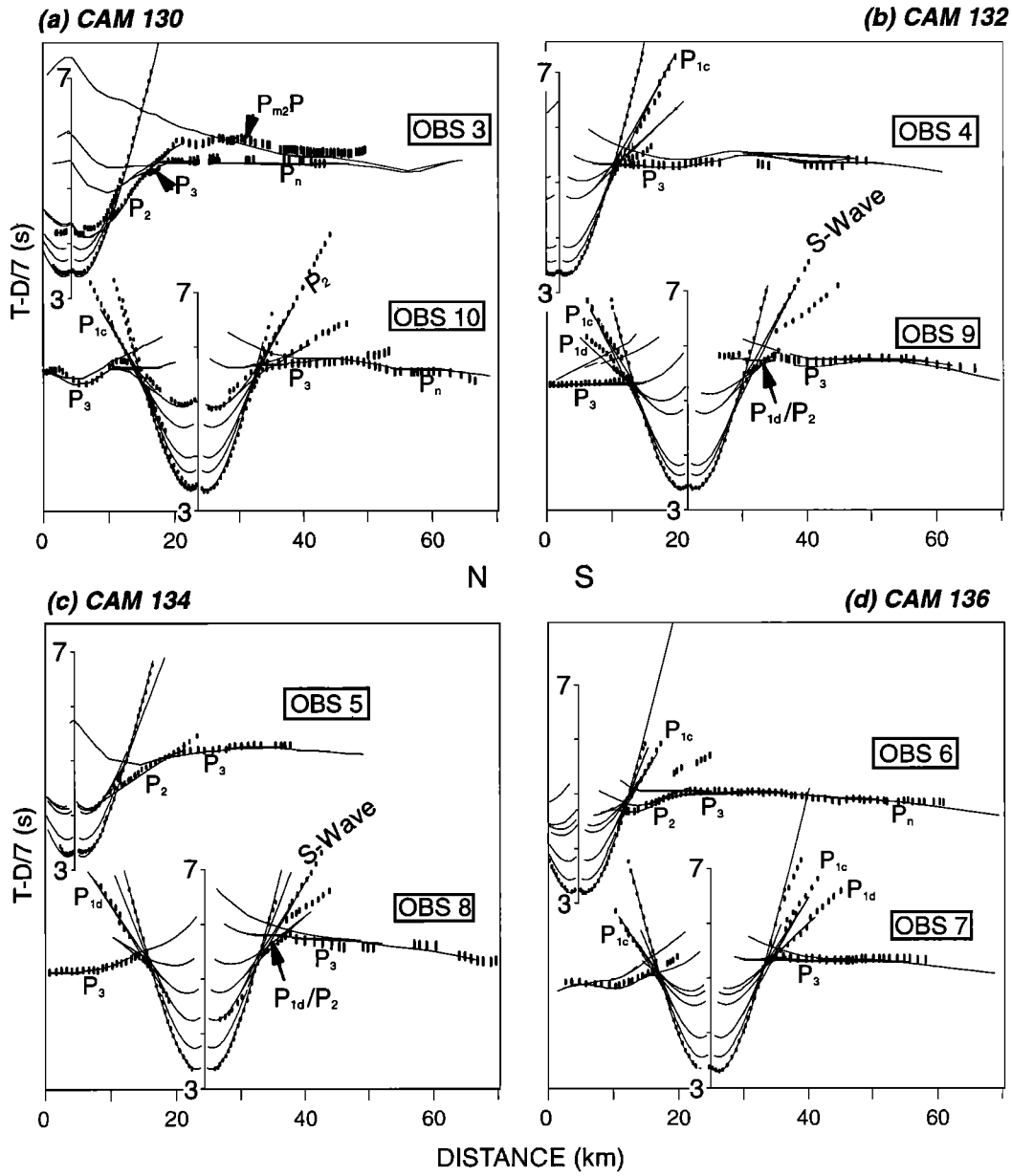

Figure 5. Picked arrival times and wide-angle record sections and computed travel time curves for the four N-S lines CAM130-136. The vertical length of each pick represents uncertainties in arrival time. Note that $P_{m2}P$ in Figure 5a is a hypothetical reflection from a mantle reflector at ~18 km depth.

~18 km, CAM134 runs along the N-S axis of a basement high. As a result, OBS 5 on CAM134 records clear P_2 as first arrivals (Figure 5c), while the southern OBS 8, located at 24 km, records a mixed phase of P_{1d} and P_2. Careful modeling shows that the basement in the north is roofed by a velocity of 4.8-5.3 km/s which is higher than the velocity of 4.2±0.2 km/s in the south (Figure 6c). This velocity range, as well as that in the lower basement layer, is in general agreement with the previous refraction line (2) of *Whitmarsh et al.* [1990], which parallels CAM134 with offset <3 km (Plate 1). For CAM136, two basement highs can be identified from reflection data. The northernmost high is not sampled by record sections of CAM136 and only modeled by the E-W line CAM144 (see section 4.2.2). The more southward basement high at ~13 km distance has been drilled at Site 900, which reveals a scattered velocity distribution in the range of 4.5-5.3 km/s [*Sawyer et al.*, 1994], slightly higher than the ridges to the west. On the same basement high, recent ODP Sites 1067 and 1068 sampled breccias, amphibolite, and serpentinized peridotite, indicating a very heterogeneous basement with a highly scattered velocity range of 2.6-6.4 km/s [*Whitmarsh et al.*, 1998]. In our data, a clear phase P_2 of OBS 6 (Figure 5d) along CAM136 samples this basement high, suggesting that the bulk velocities here, with lateral heterogeneity, increase from 4.5 to 6.5 km/s within the top 2 km of the basement (Figure 6d). Farther south on OBS 7, P_2 is not well developed, due to lack of velocity contrast at the sediment/basement boundary.

4.2.2. E-W lines. Along lines CAM142 and CAM144,

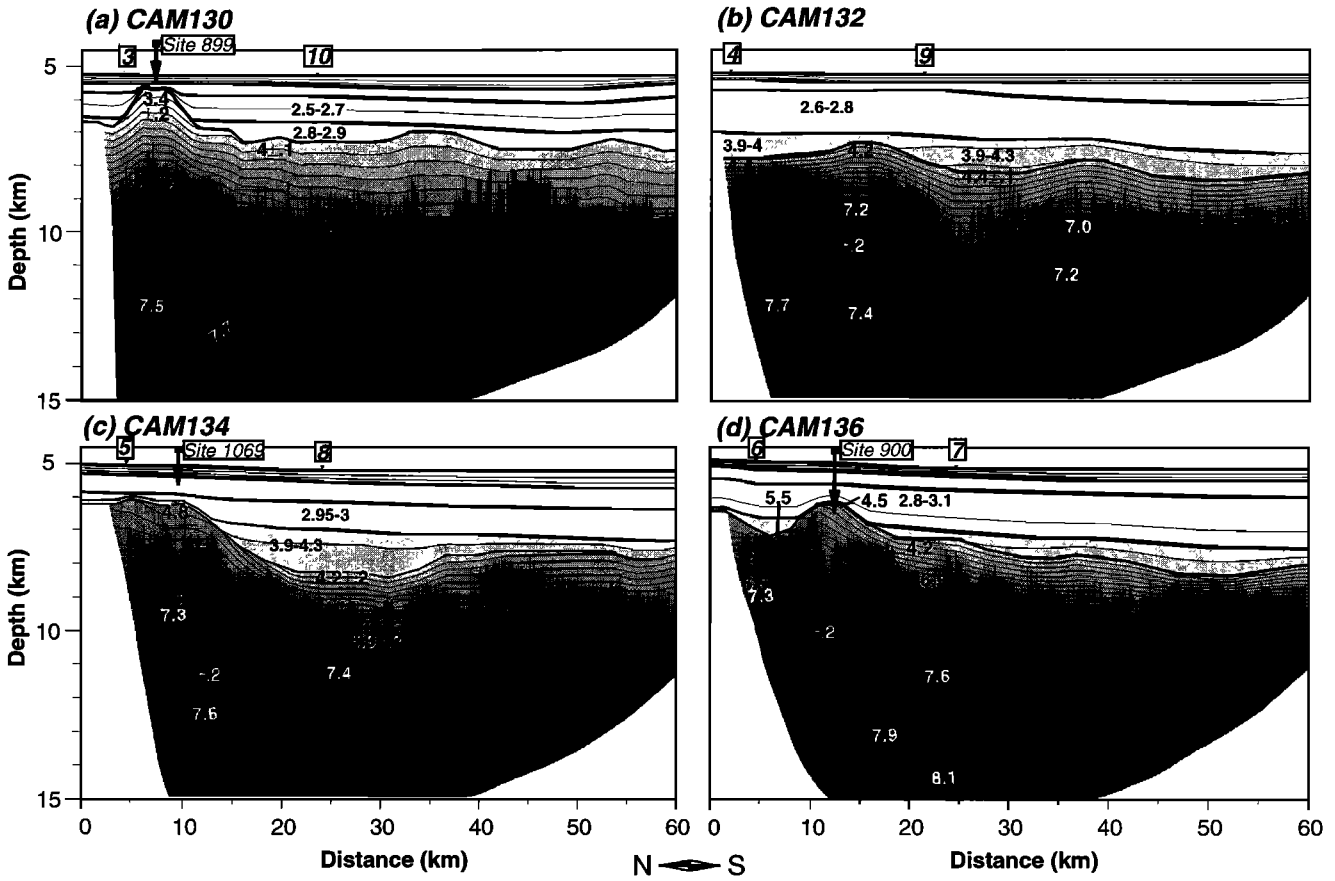

Figure 6. Velocity models for the four N-S refraction lines CAM130, CAM132, CAM134, and CAM136. OBS positions are marked by vertical triangles and labeled. Blank areas are those not covered by wide-angle rays. The contour interval of velocity is 0.2 km/s. Note the changes in basement velocity from Figures 6a to 6d.

basement highs are intersected about every 20 km (Plate 1). OBS 3, 5, and 6 along CAM144 (Figure 7) and OBS 7 along CAM142 (Figure 8) are situated on top of basement highs. In these cases, the P_2 phase is of the first type and is usually well defined. When coupled with wide-angle data from N-S lines, the velocity of the basement high is better controlled. The upper basement velocity in general increases landward, from 3.8-6.0 km/s in the west to 5.3-6.5 km/s in the east along CAM144 (Figure 9a), and from 3.5-5.2 km/s in the west to 4.2-6.7 km/s in the east along CAM142 (Figure 9b). For example, the most seaward OBS 3 on CAM144 records a P_2 phase (Figure 7) refracted from the probable peridotite basement high under ODP Site 899 (Figure 9). This OBS is on the lower part of the high observed at the northern end of CAM130 and indicates a velocity of ~3.8 km/s, which is similar to the value of 3.4 km/s to the south of the OBS (Figure 6a). Similar to the large velocity gradient observed along CAM130, the velocity beneath the high increases dramatically with depth from 3.8 to ~6 km/s.

Eastward along CAM144 at OBS 4, the P_2 phase is observed clearly on the eastern side of the OBS because of a shallowing basement between 70 and 80 km distance and is modeled as a velocity of 4.7 km/s increasing with depth to >6.5 km/s. Farther eastward at OBS 5, P_2 samples both flanks of a prominent basement high. Modeling of this phase reveals different upper basement velocities on either side: the western side is best modeled by a velocity of 5.3 km/s, while the eastern side is modeled by a velocity of <5 km/s. This indicates complexity in the velocity structure of this basement high, which may be related to sampling of different levels in a landward tilted fault block (e.g., Figure 4b). However, our limited seismic coverage does not allow us to probe the details of this complexity, and therefore we represent this basement high by the simple velocity contours shown in Figure 9a. At OBS 6 a similar vertical velocity gradient from 5.3 to 6.5 km/s is obtained by modeling P_2 (Figures 7 and 9a).

CAM142 is situated 20 km south of, and parallel to, CAM144 (Plate 1). On both sides of OBS 10, the basement relief in this southern line is less severe and mostly well imaged by the coincident reflection profile. A P_2 phase (Figure 8) is modeled by an upper basement velocity of 4 km/s that decreases eastward to 3.5 km/s beneath the basement high at 57 km distance (Figure 9b). At OBS 8 and 9, the P_2 phase is not well defined due to lack of a clear velocity contrast with the thickened sediment layer. The most eastern OBS 7 (Figure 8), however, is situated on a flank of a basement high and records a clear P_2 phase that indicates basement velocities of 4.2-6.6 km/s.

4.3. Lower Basement Layer and Upper Mantle

Along the two E-W lines (CAM142 and CAM144), the top of the lower basement layer is characterized by an unusually

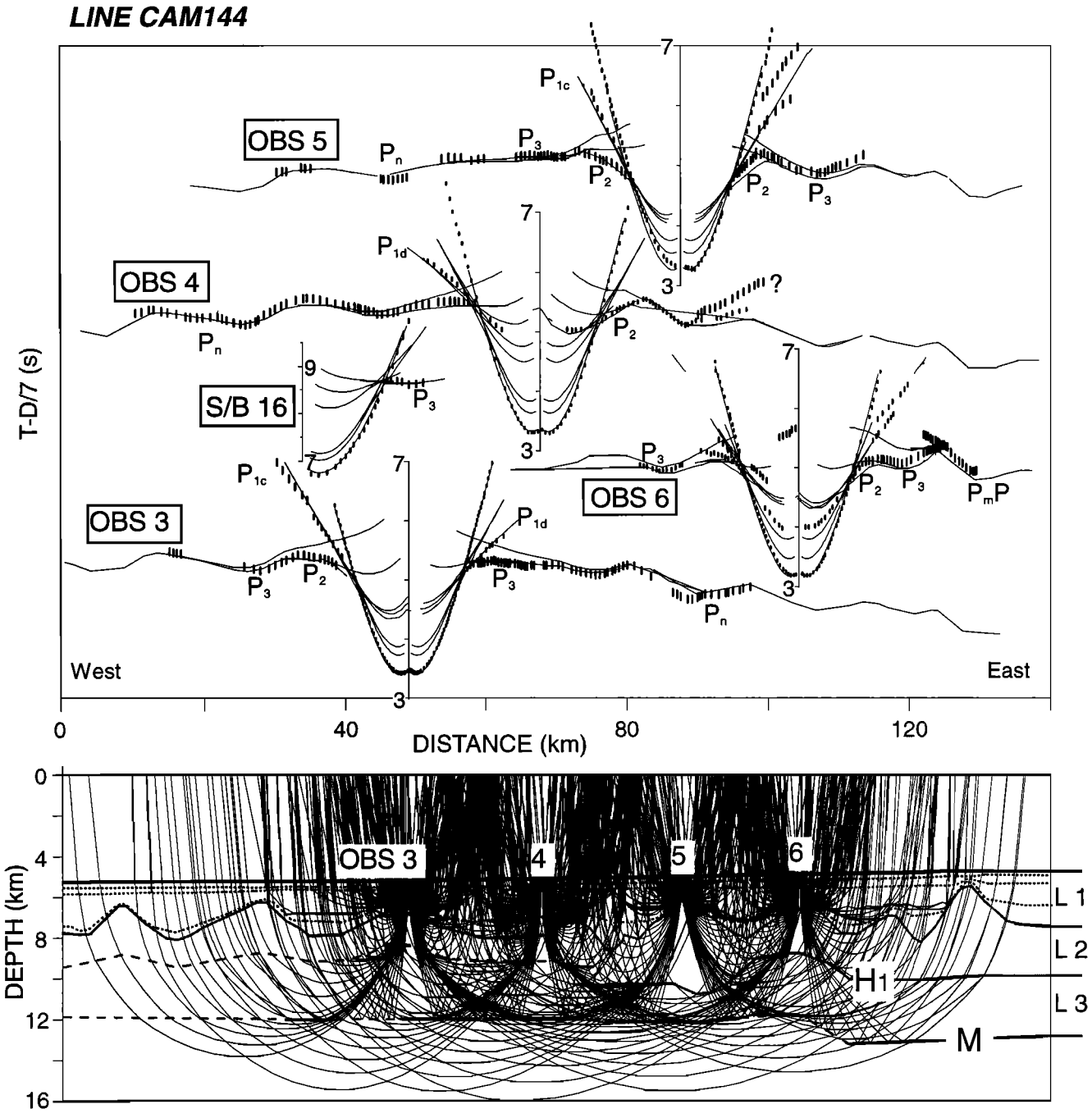

Figure 7. (top) Picked arrival times and computed travel time curves for the four OBS 3-6 on line CAM144, and (bottom) the velocity model layers with selected ray paths for generating the travel time curves. L1, L2, and L3 are sediment and upper and lower basement layers, respectively. M is Moho.

high velocity (7.3-7.9 km/s) in the eastern part, compared with a velocity of 6.4-7.5 km/s in the western part (Figure 9). On the eastern part of CAM144, the high velocity of 7.3-7.9 km/s in the lower basement is required for modeling of P_3 at OBS 5 and 6 and P_mP at OBS 6 on CAM144 (Figure 7). This velocity remains nearly unchanged to the south along CAM142, as indicated by P_3 at OBS 7, 8, and 9 and P_mP at OBS 8 (Figure 8), as well as P_3 along the crossing N-S lines CAM134 and CAM136 (OBS 8 in Figure 5c and OBS 7 in Figure 5d). The strong reflector, H_1 in Figure 4b, coincides with the boundary between the >7.2 km/s lower basement and a much reduced velocity in the upper basement on CAM144. This boundary appears to be similar to the H reflector as imaged by *Krawczyk et al.* [1996] along the nearby MCS line LG-12 (Figure 3) [*Beslier*, 1996].

The velocity of lower basement (mainly constrained by P_3) decreases westward of 70 km distance on both E-W profiles, with the most dramatic change occurring over a <20-km-wide narrow region (1) between OBS 3 and 4 on CAM144 (Figure 9a) and (2) under OBS 9 on CAM142 (Figure 9b). The N-S line CAM132 connects OBS 4 and 9 on top of this narrow region, although it is not exactly parallel to its N-S trend. Therefore

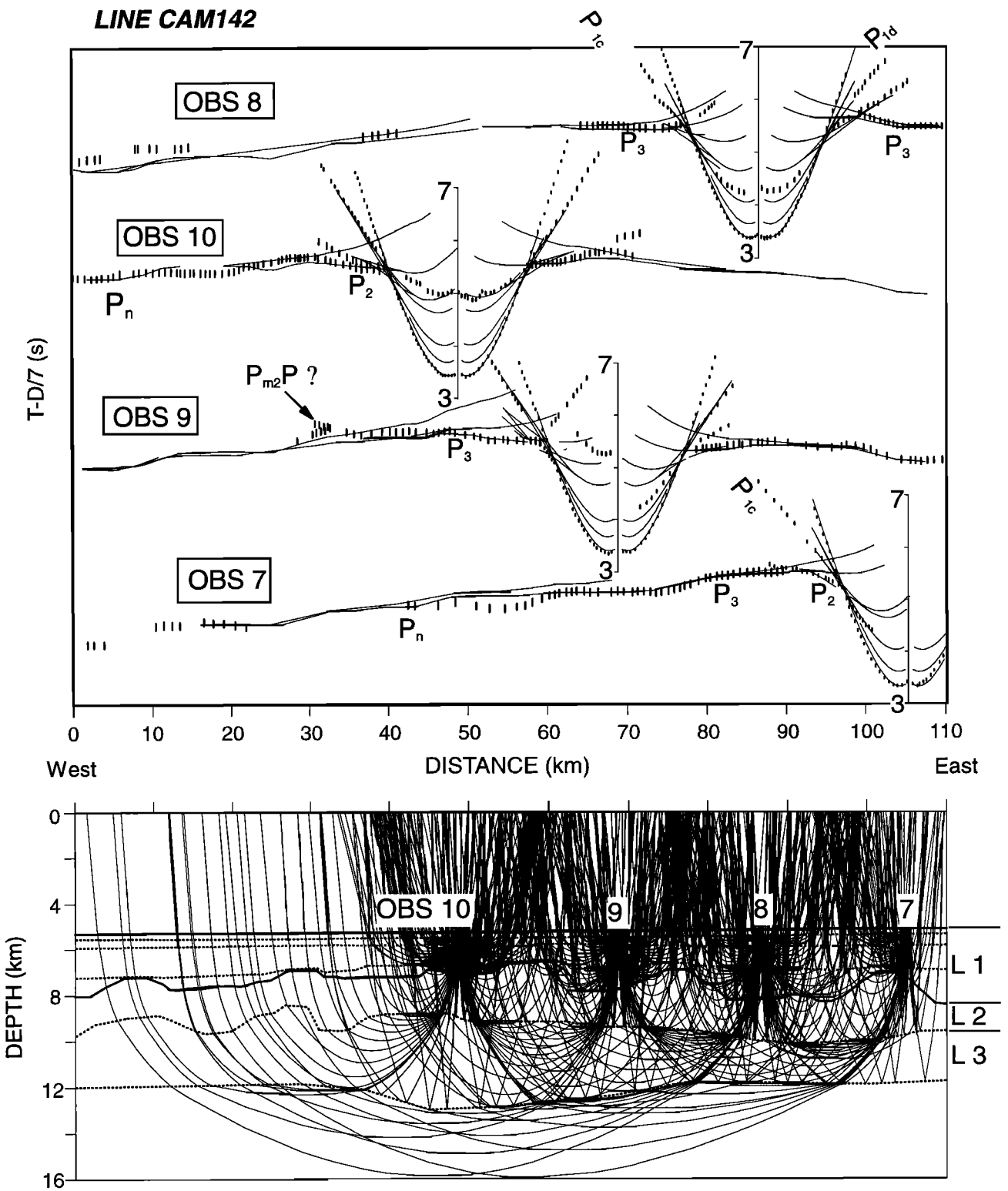

Figure 8. (top) Picked arrival times and computed travel time curves for the four OBS 7-10 on line CAM142, and (bottom) the velocity model layers with selected ray paths for generating travel time curves. L1, L2, and L3 are sediment and upper and lower basement layers, respectively. M is Moho.

CAM132 records N-S changes in lower basement velocity (Figure 6b) from 7.2-7.4 in the north (modeled from P_3 of OBS 4 and the northern side of OBS 9, Figure 5b) to 7.0-7.4 km/s southward (modeled from the much delayed P_3 at the southern side of OBS 9).

Along the westernmost line (CAM 130), the lower basement velocity is further reduced to 6.5-7.5 km/s. This is constrained by the travel time curve of P_3 on OBS 3 and 10 (Figure 5a). We note that here a relatively large velocity contrast exists between the upper and lower basement, causing

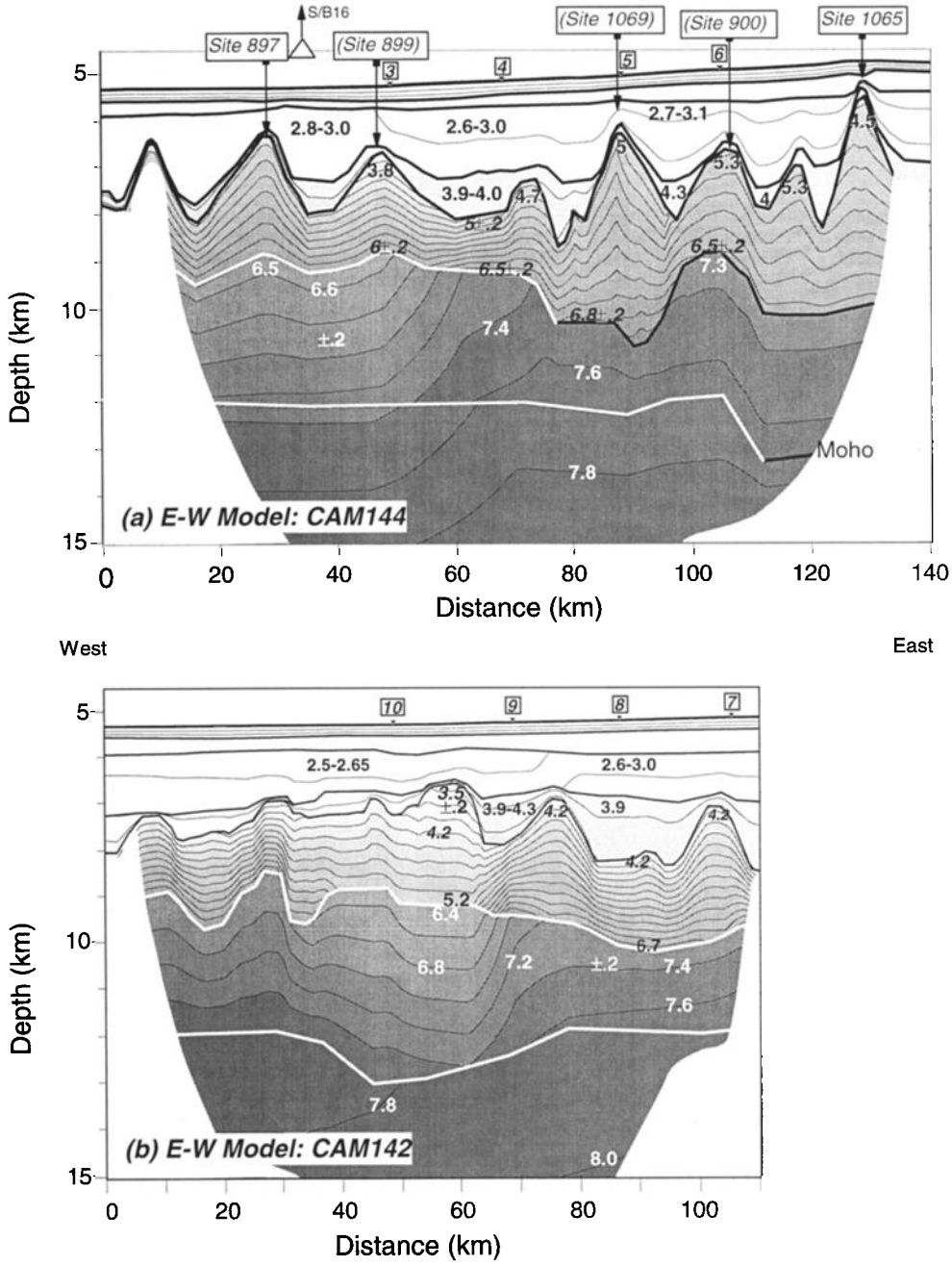

Figure 9. Velocity models for (a) CAM144 and (b) CAM142. OBS positions are marked by small triangles and labeled. Large triangle in Figure 9a shows surface position of S/B 16. Bold lines are boundaries used during modeling, with white lines associated with no major velocity contrasts. Blank areas are those not covered by wide-angle rays. The contour interval of velocity is 0.2 km/s. Note the westward decreases in crustal velocities in both Figures 9a and 9b.

a significant change in slope of seismic phases P_2 and P_3. For example, OBS 10 records the largest P_2/ P_3 slope change, best modeled as a velocity jump from 5.2 to 6.5 km/s south of the OBS (Figure 6). This jump in velocity cannot be deduced from E-W profiles, as in these profiles P_2 and P_3 cannot be clearly separated from other arrivals (e.g., OBS 3 on CAM144 in Figure 7a and OBS 10 on CAM142 in Figure 8a).

The westward reduction of velocity within the lower basement and the lack of P_mP under CAM130 imply a large downward velocity gradient. Modeling of the P_3/P_n phases suggests a gradient from 6.5 to 8.0 km/s at ~15 km depth, where the velocity approaches a typical mantle velocity of ~8.0 km/s. Such a high-velocity gradient is also supported by data from S/B 16 (Figure 7), where arrival P_3 can be clearly identified and modeled. From coincident reflection profiles it is clear that farther seaward at 0-35 km distance on CAM142 and CAM144, there are further complications within the lower basement. Although we have managed to grossly model the lower basement arrivals of OBS 3 and 10, further refinements would require additional data to the west.

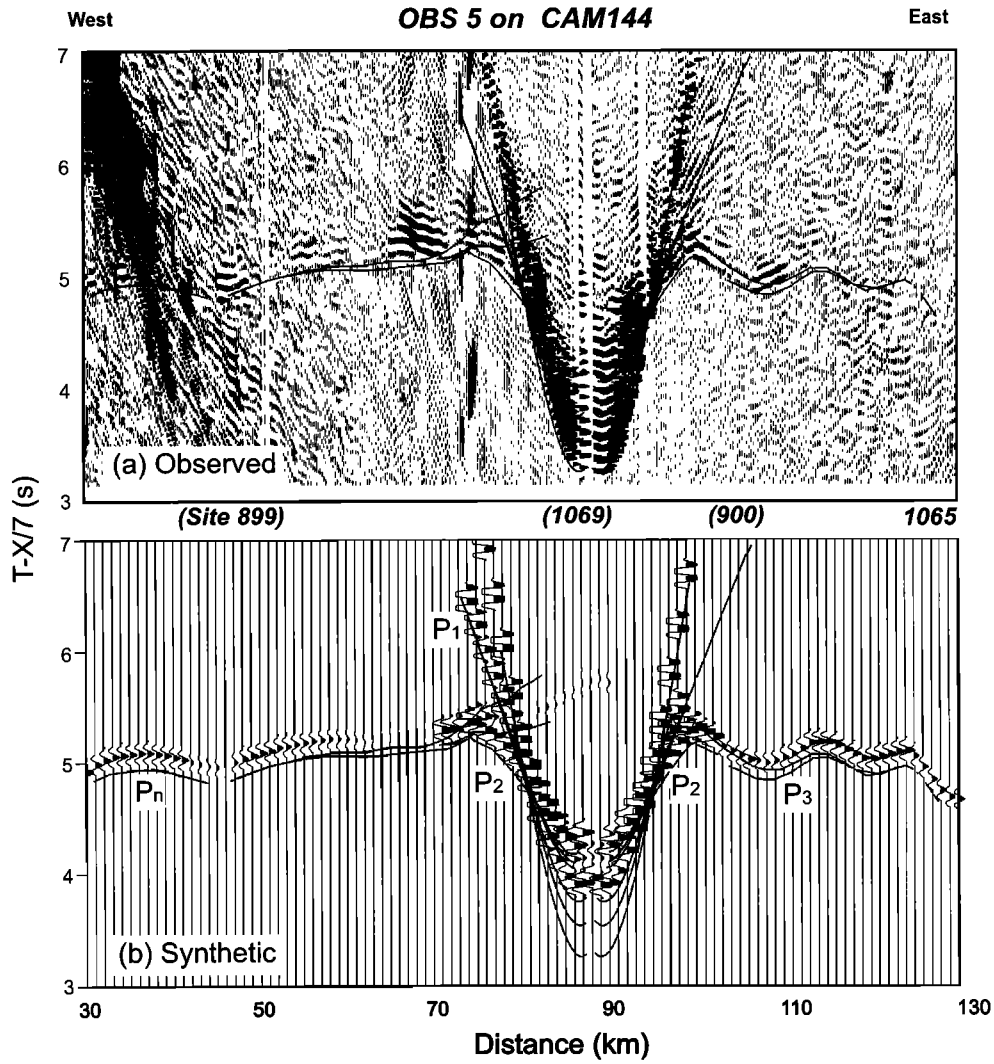

Figure 10. (a) Observed and (b) synthetic record sections of OBS 5 on CAM144. The amplitudes of water waves and reflections from the first sediment layer are not modeled. For synthetic modeling details, refer to section 4.4.

In all of the study area except the most northeastern part (Figure 9), we see an absence of a clear velocity contrast between basement and mantle which would normally be found at the Moho. Instead, the velocity in the lower basement, which is highly variable from east to west and more uniform in the N-S direction, gradually increases downward to ~8.0 km/s at about 14-15 km depth. This absence of clear Moho is consistent with earlier refraction data [*Whitmarsh et al.*, 1990] and MCS reflection data [e.g., *Pickup et al.*, 1996] in the region.

A hypothetical sub-Moho reflector, $P_{m2}P$, is clearly observed by OBS 3 (Figure 5a) along the CAM130 line. This phase can be modeled by inserting a deep reflector at ~18 km depth in the velocity model of Figure 6a. However, this $P_{m2}P$ phase is not identified on any other wide-angle profiles in the study area, and even along the same CAM130 line, a corresponding reflector does not exist along the MCS reflection profile (not shown). This region is at the northern limit of the overlap zone between peridotite ridges R3 and R4 (Figure 2), so it might be expected to have a complex structure. Therefore, our models in Figure 6 do not include this reflector and its origin (offline reflector?) requires further study.

4.4. Amplitude Modeling and Resolution

Synthetic seismograms were generated using a geometrical ray theory for inhomogeneous structures [*Zelt and Forsyth*, 1994]. A Poisson's ratio of 0.25 is assumed for all layers except the water layer where the ratio is assumed as 0.5. Density of the water layer is set to be 1.0 g/cm^3, while densities in g/cm^3 of all other layers are assumed by the relationship $\rho = -0.6997 + 2.2302\ v - 0.598\ v^2 + 0.07036\ v^3 - 0.0028311\ v^4$, where v is P wave velocity [*Ludwig et al.*, 1970]. The source wavelet was a 29-point low-pass Ricker wavelet centered at a frequency of 6 Hz. Figure 10 shows a comparison of observed and synthetic seismograms for OBS 5 on CAM144 generated from the model in Figure 9a. It can be seen that the synthetic seismograms simulate reasonably well the observed phases from sediment, basement and mantle (i.e., P_1, P_2, P_3, and P_n). One exception is the misfit of amplitudes at 65-70 km distance west of OBS 5 where the defocusing of refracted seismic energy from the lower basement layer, caused

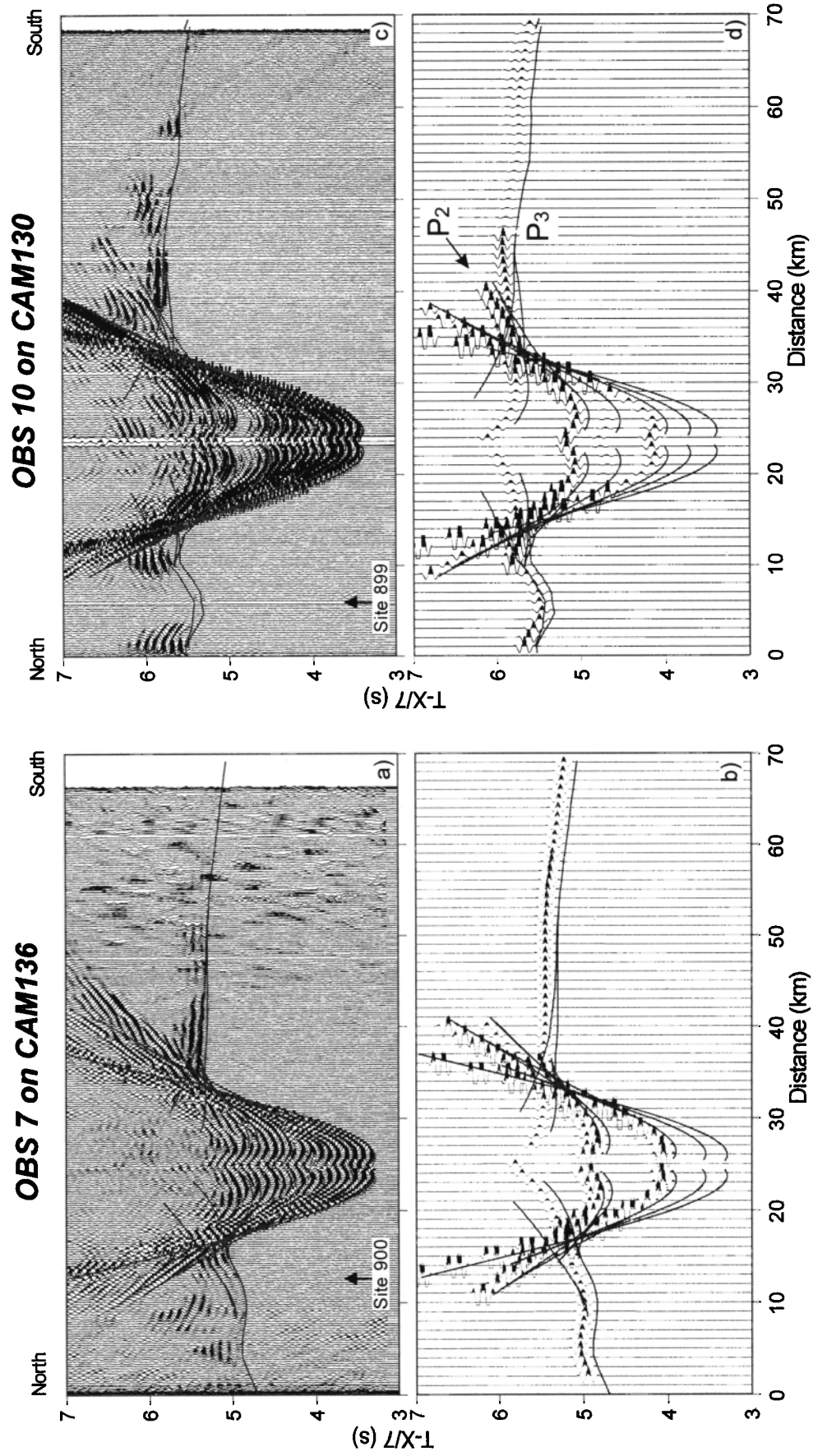

Figure 11. (a) Record section of OBS 7 along CAM136; (b) synthetic seismograms for Figure 11a generated from the model shown in Figure 6d; (c) record section of OBS 10 along CAM130; and (d) synthetic seismograms for Figure 11c generated from the model shown in Figure 6a. Refer to caption of Figure 10 for other details.

by severe basement relief and heterogeneous velocity structure of basement between Sites 899 and 1069 (Figure 9), significantly reduces the computed amplitudes. This problem is reduced in the N-S direction due to larger wavelength of basement relief, resulting in better fit between computed and observed amplitudes (e.g., OBS 7 in Figures 11a and 11b). The flatter basement topography along this direction also allows a clear separation of P_2 and P_3 phases that are well modeled for OBS 10 along CAM130 in Figures 11c and 11d. In figures 11c and 11d the basement high at Site 899 again diffracts a significant amount of energy of P_2/P_3. On the other hand, we note that it is generally much easier to model the travel time curves than the amplitudes in cases of the complicated velocity structures shown in Figures 6 and 9. Velocity-depth models in this paper are primarily determined by forward modeling of the observed travel times.

In the error analysis of model parameters we fix the depth to basement that is determined by coincident reflection profiles. We then perturb the velocity values for a few less complicated locations within the upper basement. The error bounds are then determined when the maximum allowable misfits to the observed travel time curves were reached. Our velocity models are accurate only for the northern 50 km on the N-S models shown in Figure 6, although the observed wide-angle data extend for an additional 20 km to the south. At these southern distances our ray coverage is too sparse to accurately define the basement velocities, which are complex, as suggested by basement reflective patterns and comparison to velocity models along IAM-9 [*Discovery 215 Working Group*, 1998].

For the northern 50 km of our models the uncertainties obtained for the velocity of the lower basement layer are found to be no greater than ±0.2 km/s in all cases. For the upper basement the uncertainty of velocity is sometimes improved to ±0.1 km/s when P_2 is clearly observed in both N-S and E-W directions. An exception to this occurs when P_2 is near a basement high and the velocity uncertainty is degraded to ±0.2 km/s. The situation for OBS 7 is complicated by its proximity to a basement high with a large vertical velocity gradient, and by the absence of clear energy along the N-S direction. Perturbing the basement velocity suggests a degraded velocity uncertainty of ±0.2 km/s. OBS 8 has a combined P_{1d}/P_2 observed along both the N-S and E-W directions, caused by the thick sediment layer 1d, with velocities similar to the basement. To estimate the possible uncertainties, we jointly perturbed velocities associated with both P_2 and P_{1d}, which results in an uncertainty of ±0.2 km/s.

No error analysis was undertaken for the depths of subbasement boundaries of the model because they do not generally correspond with major changes in velocity. In particular, a clear Moho discontinuity is only observed in a narrow (<10 km) region on the easternmost end of CAM144. In this region, the midbasement boundary is also associated with a major velocity change, primarily constrained by travel times of a major midbasement reflector in MCS profiles. A more complete analysis of this feature requires use of the complete MCS reflection coverage with the velocity model, which will be focus of a subsequent paper.

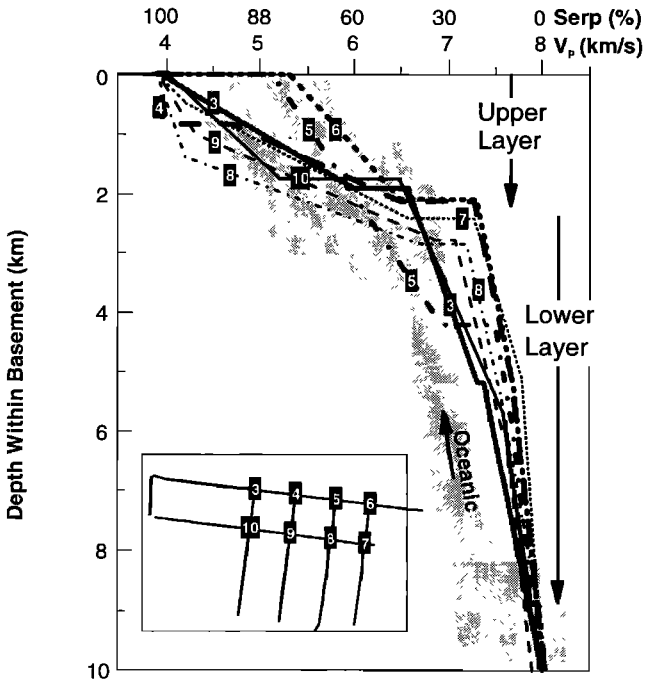

Figure 12. Compilation of *P* wave velocity-depth profiles within basement under OBS 3-10. Shaded area indicates bounds for 59-170 Ma Atlantic crust [*White et al.*, 1992]. Note the thickened upper crust under OBS 5 caused by its sitting atop a basement high. Serp, percent of serpentinization (data from *Christensen* [1966, 1972]).

5. Discussion

5.1. Geological Interpretation of Velocity Models

In Figure 12, the general features of our velocity models are shown as a series of 1-D velocity-depth functions, which are derived from the 2-D models (Figures 6 and 9) beneath each OBS at the eight intersection points of the two E-W and four N-S profiles. None of these 1-D models fits within the bounds of typical oceanic crust [e.g., *White et al.*, 1992] nor are they consistent with oceanic crust formed at very slow spreading rates for the following reasons:

1. All models contain a lower basement layer ~5 km thick with velocities well in excess of normal oceanic layer 3. The high velocities within the layer gradually approach a mantle velocity of 8 km/s at subbasement depths of ~10 km, without a well-defined Moho. These models lie well outside the bounds of normal ocean crust. In addition, oceanic crust formed at very slow spreading rates [e.g., *Muller et al.*, 1997; *Osler and Louden*, 1995; *Grevemeyer et al.*, 1997], though thinner than normal ocean crust consistently exhibits both a distinct oceanic layer 3 (V_p < 7.0-7.2 km/s) and clear Moho signatures, unlike the lower crustal models shown in Figure 12.

2. All models, except for OBS 5 and 6, contain an ~2-km-thick upper basement layer with high-velocity gradients and very low topmost basement velocities of ~4 km/s. These velocities are lower than values observed in the oceanic upper crust of >5.6 km/s west of Galicia Bank [*Whitmarsh et al.*, 1996] and of ~4.5 km/s at the western end of line IAM-9 (S. Dean, personal communication, 1998). These upper basement velocities are also too low, and the gradients are too high, for typical velocity models of the Iberian continental crust [*Iberian Lithosphere Heterogeneity and Anistropy Deep Seismic Sounding (ILIHA DSS) Group*, 1993].

These comparisons confirm previous suggestions that the OCT in the southern Iberia Abyssal Plain does not dominantly consist of either thin oceanic or thinned continental crust [*Pickup et al.*, 1996; *Brun and Beslier*, 1996; *Discovery 215 Working Group*, 1998], in disagreement with earlier interpretations based on more sparse refraction profiles [*Whitmarsh et al.*, 1990, 1993]. This conclusion is also consistent with the absence of significant oceanic basalt in ODP cores [*Sawyer et al.*, 1994; *Whitmarsh et al.*, 1998] and with the presence of low amplitude magnetic anomalies observed within the OCT east of R3 (Plate 1), which can not be modeled by slow or ultraslow seafloor spreading [*Whitmarsh and Miles*, 1995; *Whitmarsh et al.*, 1996].

An alternative interpretation is that the basement in the OCT is primarily serpentinized upper mantle peridotites [*Boillot et al.*, 1989; *Pickup et al.*, 1996]. Conversion of seismic velocity to degree of serpentinization in Figure 12 is made using laboratory measurements on ophiolite samples [*Christensen*, 1966] and on samples from the Mid-Atlantic Ridge [*Christensen*, 1972]. This conversion yields values >95% for the serpentinization of the basement immediately beneath the ridges in the western part of our survey area and values of ~60% for the degree of serpentinization at the bottom of the upper basement layer (at ~2 km below basement surface). These values are generally consistent with results of ODP drilling: (1) at Site 897 [*Sawyer et al.*, 1994], where rock samples are 80-100% serpentinized and velocities of 2.8-5.3 km/s were measured; (2) at Site 899 [*Sawyer et al.*, 1994], where heavily serpentinized peridotite breccias were also sampled and velocities of 3.4-5.1 km/s were measured; and (3) at Site 1068 [*Whitmarsh et al.*, 1998], where 80-95% serpentinized fractured peridotites had velocities of 2.7-4.6 km/s. A similar comparison for the lower basement layer suggests values of 0-25% serpentinization beneath the eastern section of the survey and 25-45% beneath the far western region.

Velocity-depth models of the upper basement layer for OBS 5 and 6 are clearly different from those at the other OBS positions (Figure 12). Much higher values of 5.0-5.4 km/s are observed for top basement velocities and the velocity gradients are much lower. At OBS 5 we also observe a much greater thickness for the upper basement layer. We interpret this basement layer in the northeastern sector of our survey (i.e., along CAM144 east of OBS 4) as thinned continental crust, based on the following reasons: (1) ODP Sites 901, 1065, and 1069 [*Sawyer et al.*, 1994; *Whitmarsh et al.*, 1998] drilled sediments that were deposited in shallow water marine environments, suggesting a continental origin for the underlying basement; (2) the higher basement velocities east of OBS 4 are similar to velocities >5.8 km/s in the upper continental crust beneath the western Iberian Peninsula [*Córdoba et al.*, 1988; *ILIHA DSS Group*, 1993]; (3) MCS profiles across the same basement highs east of OBS 4 (e.g., Figure 4b) clearly suggest the presence of tilted fault blocks (Site 1065 [*Whitmarsh et al.*, 1998]), which are bounded by seaward dipping normal faults connecting to a horizontal midcrustal reflection bounding the top of the high-velocity lower basement layer. These reflections are similar to the H reflector observed in a similar location beneath LG-12 (Figure 3) [*Krawczyk et al.*, 1996] and the S reflector west of Galicia Bank observed on MCS line GP-101 [*Reston*, 1996].

The primary implication of our seismic velocity model for the OCT along the ODP transect is that very little melt is produced over a zone ~100 km wide where the continental crust has been thinned by very large (possibly infinite) stretching factors, exposing the upper mantle and leading to extensive serpentinization. Laboratory (sandbox) models of continental rifting [e.g., *Brun and Beslier*, 1996] can simulate the occurrence of this transitional region, but computer models that include the effects of melt do not [*Pedersen and Ro*, 1992; *Bown and White*, 1995]. In *Bown and White*'s [1995] 1-D model, rift durations of 15-25 m.y., consistent with data from the Iberia margin, would result in melt production of <1 km for stretching factors ß=9-15. Melt production might be further inhibited by additional factors not included in the model, such as partial extension during earlier episodes of rifting, by 2-D lateral conductive cooling, and by advective cooling due to penetration of water into the upper mantle. In addition, simple shear extension during continental rifting might also reduce the production of melt [*Latin and White*, 1990]. Our seismic models, however, are not able to distinguish the presence of small amounts of melt (with velocities of 5.6-7.0 km/s) within layers of primarily serpentinized peridotite, given the observed wide velocity range (3.8-7.8 km/s) for the serpentinites. Existence of "gabbroic" samples at the basement high drilled by Sites 900 and 1067 suggests that some melting might have occurred during rifting. In addition, the light rare earth element enrichment of the few basalt clasts recovered on Leg 149 [*Seifert et al.*, 1997] indicates low degrees of melting. However, by far the dominant rock type, in the ODP igneous basement cores from the OCT in the southern Iberia Abyssal Plain, is serpentinized peridotite, none of which contains discrete patches of melt products. However, sampling of the OCT basement is still limited to basement highs, and extensive regions of deeper basement, as well as the thicker sections of synrift sedimentary sequences, remain unsampled.

5.2. Three-Dimensional View of the Ocean-Continent Transition

In Figure 13 the correlation of velocities to rock types from the 1-D sections presented above is extended along each seismic line in order to represent a 3-D view of the basement composition of the OCT. Thinned upper continental fault blocks (unshaded area with crosses in Figure 13, top) exist only in the northeast sector of the study area, while the remaining basement is composed primarily of upper mantle peridotite which has undergone various amounts of serpentinization. The continental fault blocks are defined by linear ridges, which extend to the south from Vasco da Gama Seamount (see Figure 2 for location) on the southern edge of Galicia Bank. The termination of these fault blocks is indicated in our seismic models as a reduction of basement velocities: (1) from east to west along line CAM144 in the vicinity of OBS 4 (Figure 9a); and (2) along N-S profiles CAM136 and 134 (Figure 6), south of their intersections with CAM144.

This decrease in basement velocity is, in general, coincident with increases in basement depth at the southern termination of the N-S fault blocks. These fault blocks terminate approximately at the 4.5 km/s contour line (Figure 13, bottom). Note one exception, however, in that mafic rocks including one or more occurrences of gabbro, tonalite, amphibolite, and anorthosite were sampled at ODP Sites 900, 1067, and 1068 on a local high on a roughly N-S basement

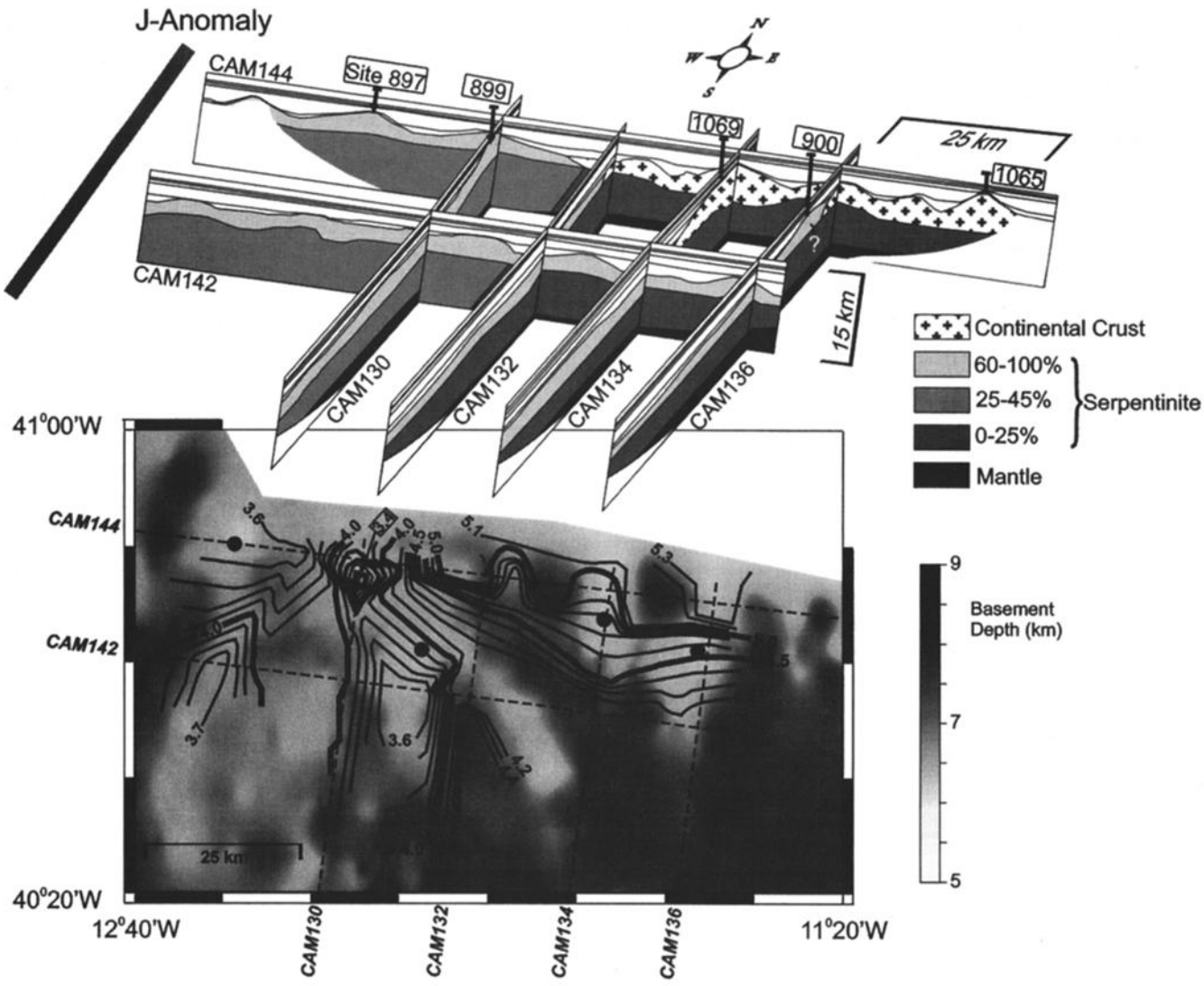

Figure 13. (top) Three-dimensional interpretation of seismic velocity models along the six refraction lines. Note the major divisions of basement within the OCT, where increased serpentinization occur beneath ridge segments in the western sector, exposed mantle is less serpentinized in the eastern sector, and thinned continental crust remains only in the northeast beneath a series of N-S lineated fault blocks. Question marks (?) at Site 900 indicate debatable interpretation. (bottom) Velocity contours of the topmost basement based on results from six profiles of Figures 6 and 9. Offline contours are extrapolated based on topographical trend of the depth-to-basement map in Plate 1. Contours interval is 0.1 km/s.

ridge along line CAM136 immediately south of line CAM144. Basement velocities in this region along CAM136 show a strong north-south gradient across the elevated basement high, which is not well resolved by the limited OBS data in the presence of severe basement topography. This suggests a complex 3-D structure that requires more detailed wide-angle data to resolve. However, since the geometry of the basement block appears similar to the continental block seaward at Site 1069, our 3-D fence diagram in Figure 13 (top) interprets the basement here as continental.

South of the continental blocks, the continental crust is replaced by an upper layer of highly serpentinized peridotite, as observed along CAM142, where evidence for significant block faulting is absent and velocity in the topmost basement decreases to 4.2 km/s from values of 5.3 km/s along the eastern part of CAM144. This layer may be the same as the unreflective layer observed along the MCS seismic line IAM-9 south of our study area, which *Pickup et al.* [1996] suggested was created by vigorous penetration of seawater down a cracking front, leading to extensive serpentinization that destroyed any preexisting reflective fabric. The lower boundary of this layer marked the depth of penetration of this cracking front, below which seawater penetrated more gradually with decreasing amounts of serpentinization. In this case, our velocity analysis suggests that the amount of serpentinization decreases substantially from 60-100% in the upper layer to 0-25% in the lower layer.

Approximately at the position of line CAM132, the basement depths and velocity models suggest further changes in basement structure from east to west. In particular, a

westward decrease in velocity is evident in both basement layers: (1) at the top of basement from 4.7 to 3.8 km/s along CAM144 and from 4.2 to 3.5 km/s along CAM142 and (2) within the lower basement layer on both lines CAM144 and CAM142 from 7.2-7.7 km/s in the east to 6.4-7.2 km/s in the west. This change is coincident with the elevated basement topography (Figure 13) in the western half of the study area, where highly serpentinized peridotites have been drilled at ODP Sites 897 and 899. Thus we suggest that the degree of serpentinization of the exposed upper mantle peridotites intensified during final rifting to form the basement ridges west of CAM132. Seafloor spreading is expected to occur to the west of this region between R3 and the J anomaly (Figure 2 and Plate 1). Our velocity models do not define this transition. We note, however, that the previous refraction lines 3 and 4 [*Whitmarsh et al.*, 1990] indicate a major discontinuity in the vicinity of the R3 basement ridge at the western end of our E-W profiles (Plate 1 and Figure 13). The velocity structure west of this ridge is clearly oceanic in character, with well developed oceanic layer 2 (v=5.4 km/s) and layer 3 (v=6.8-7.2 km/s) and almost standard thickness of ~6 km, while the velocity structure to the east agrees well with our serpentinite model beneath ridge R3.

In summary, our velocity models indicate both north-south and east-west variations across the southern Iberia Abyssal Plain. North-south variations are caused by the termination of the rifted continental fault blocks south of Galicia Bank; east-west variations are caused by the increase in serpentinization of exposed upper mantle before initial formation of oceanic crust. The boundaries of these major variations are relatively abrupt zones where complex structures may occur. The existence of a broad, but variable-width, zone of serpentinized peridotite basement between thinned continental and normal (or slightly thin) oceanic crust is similar to structures observed across the Labrador and West Greenland conjugate margins [*Chian and Louden*, 1994; *Chian et al.*, 1995b]. However, in these cases the outer zone of increased serpentinization seems to be either absent, or limited in extent and not well resolved by the more limited seismic data coverage [*Keen et al.*, 1994; *Chalmers and Laursen*, 1995].

6. Conclusions

Basement velocity models have been derived from an intersecting grid of two E-W and four N-S wide-angle reflection/refraction profiles in the southern Iberia Abyssal Plain, south of Galicia Bank. This unusually wide transition zone between oceanic and continental crust has previously undergone extensive investigation, including a transect of ocean drilling boreholes, but the nature of its deeper basement structure has remained elusive. Analysis of our velocity models results in a new 3-D view of structure within the ocean-continent transition (OCT, Figure 13) from which we are able to make the following interpretations:

1. Thinned upper continental crust 2-5 km thick with velocities 5.0-6.6 km/s is limited to a series of N-S fault blocks immediately south of Galicia Bank. The crust is underlain by a lower high-velocity layer of weakly serpentinized (i.e., 0-25%) peridotite, which exists throughout the eastern part of the survey area. There is a sharp contrast in velocity at the base (~9 km depth) of the continental crust, but there is no well-defined Moho at the base of the high-velocity lower basement layer, where velocities gradually approach a normal mantle velocity of ~ 8 km/s at a subbasement depth of ~10 km.

2. Basement within the OCT dominantly consists of a broad region of previously exposed upper mantle that has been serpentinized by variable amounts both vertically and horizontally. In the southeast sector of our survey where basement topography deepens and becomes subdued, continental fault blocks are replaced by an upper layer of more pervasively serpentinized (i.e., 25-45%) peridotite. Low basement velocity and high vertical velocity gradient (from 4.2 to 6.7 km/s) characterize this ~2-km-thick layer, which probably corresponds to a seismically unreflective layer, previously identified along MCS profile IAM-9 to the south of our survey.

3. In the western section of our survey beneath a series of elevated basement ridges, velocities in basement layer reduce to 3.5-6.0 km/s and in the lower layer reduce to 6.4-7.5 km/s. These changes suggest that both upper and lower layers have become more highly serpentinized (with values of 60-100% in the upper layer and 25-45% in the lower layer) beginning during the last stages of rifting and immediately before formation of oceanic crust.

4. Typical oceanic crust does not exist within the survey region. The beginning of seafloor spreading is not well defined by existing seismic data but lies east of the magnetic J anomaly and west of the peridotite ridge R3 sampled by ODP Site 897.

5. Lateral variations in basement velocity structure primarily occur across relatively narrow (<20 km) boundaries where complex variations may occur. Details of these variations within these transition regions are not well defined by our data and require additional wide-angle seismic data.

Acknowledgements. This work was supported by grants from the U.K. Natural Environment Research Council (grant GR3/9354 to T.A.M. and R.B.W.) and the Natural Sciences and Engineering Research Council of Canada (grant CSP0149983 to K.E.L.). We thank S. Dean for processing all the Cambridge OBS data, and the officers and crew of the RRS *Discovery*, technical assistance from the Research Vessel Services, and scientific participants in *Discovery* cruise 215 for their expert help at sea. Operations of the ocean bottom seismometers were led by T. Owen and R. Smith (Cambridge University), R. Iuliucci (Dalhousie University), and D. White (Southampton Oceanography Centre). S. Corrie assisted with initial processing of the Dalhousie OBS data. T.A.M. was supported by a Royal Society University Research Fellowship. G. Boillot kindly supplied the LG-12 digital seismic data.

References

Beslier, M.-O., Data report: Seismic line LG-12 in the Iberia Abyssal Plain, *Proc. Ocean Drill. Program, Sci. Results, 149*, 737-739, 1996.

Beslier, M.-O., M. Ask, and G. Boillot, Ocean-continent boundary in the Iberia Abyssal Plain from multichannel seismic data, *Tectonophysics, 218*, 383-393, 1993.

Boillot, G., and E.L. Winterer, Drilling of the Galicia margin: Retrospect and prospect, *Proc. Ocean Drill. Program, Sci. Results, 103*, 809-828, 1988.

Boillot, G., S. Grimaud, A. Mauffret, D. Mougenot, J. Kornprobst, J. Mergoil-Daniel, and G. Torrent, Ocean-continent transition off the Iberian margin: A serpentinite diapir west of Galicia Bank, *Earth Planet. Sci. Lett., 48*, 23-34, 1980.

Boillot, G., J., G. Feraud, M. Recq, and J. Girardeau, "Undercrusting" by serpentinite beneath rifted margins: The examples of the west Galicia margin (Spain), *Nature, 341*, 523-525, 1989.

Bown, J. W., and R. S. White, Effect of finite extension rate on melt generation at rifted contiental margins, *J. Geophys. Res., 100*, 18011-18029, 1995.

Brun, J.P., and M.-O. Beslier, Mantle exhumation at passive margins, *Earth Planet. Sci. Lett., 142,* 161-173, 1996.

Chalmers, J.A., and K.H. Laursen, Labrador Sea: The extent of continental and oceanic crust and the timing of the onset of seafloor spreading, *Mar. Pet. Geol., 12,* 205-217, 1995.

Chian, D., and K.E. Louden, The structure of Archean/Ketilidian crust along the continental shelf of southwestern Greenland from a seismic refraction profile, *Can. J. Earth Sci., 29,* 301-313, 1992.

Chian, D., and K.E. Louden, The continent-ocean crustal transition across the southwest Greenland margin, *J. Geophys. Res., 99,* 9117-9135, 1994.

Chian, D., C. E. Keen, I. Reid, and K.E. Louden, Evolution of non-volcanic rifted margins: New results from the conjugate margins of the Labrador Sea, *Geology, 23,* 589-592, 1995a.

Chian, D., K.E. Louden, and I. Reid, Crustal structure of the Labrador Sea conjugate margin and implications for the formation of nonvolcanic continental margins, *J. Geophys. Res., 100,* 24239-24253, 1995b.

Christensen, N.I., Elasticity of ultramafic rocks, *J. Geophys. Res., 71,* 5921-5931, 1966.

Christensen, N.I., The abundance of serpentinites in the oceanic crust, *J. Geol., 80,* 709-719, 1972.

Córdoba, D., E. Banda, and J. Ansorge, *P*-wave velocity-depth distribution in the Hercynian crust of northwest Spain, *Phys. Earth Planet. Inter., 51,* 235-248, 1988.

Dean, S.M., C.M. Krawczyk, and T.A. Minshull, Prestack depth migration of seismic reflection profiles, *Proc. Ocean Drill. Program, Initial Rep., 173,* 157-161, 1998.

Discovery 215 Working Group (T. Minshull, S.M. Dean, R.B. Whitmarsh, S.M. Russel, K.E. Louden, and D. Chian), Deep structure in the vicinity of the ocean-continent transition zone under the southern Iberia Abyssal Plain, *Geology, 26,* 743-746, 1998.

Féraud, G., M.-O. Beslier, and G. Cornen, $^{40}Ar/^{39}Ar$ dating of gabbros from the ocean/continent transition of the western Iberia margin: Preliminary results, *Proc. Ocean Drill. Program, Sci. Results, 149,* 489-495, 1996.

Grevemeyer, I., W. Weigel, R.B. Whitmarsh, F. Avedik, and G. Ali Deghani, The Aegir Rift: Crustal structure of an extinct spreading axis, *Mar. Geophys. Res., 19,* 1-23, 1997.

Horsefield, S.J., R.B. Whitmarsh, R.S. White, and J.-C. Sibuet, Crustal structure of the Goban Spur passive continental margin: Results of a detailed seismic refraction survey, *Geophys. J. Int., 119,* 1-19, 1994.

Iberian Lithosphere Heterogeneity and Anisotropy Deep Seismic Sounding (ILIHA DSS) Group, A deep seismic sounding investigation of lithospheric heterogeneity and anisotropy beneath the Iberian Peninsula, *Tectonophysics, 221,* 35-51, 1993.

Keen, C.E., P. Potter, and S.P. Srivastava, Deep seismic reflection data across the conjugate margins of the Labrador Sea, *Can. J. Earth Sci., 31,* 192-205, 1994.

Klitgord, K.D., and H. Schouten, Plate kinematics of the central Atlantic, in *The Geology of North America,* vol. M, *The Western North Atlantic Region,* edited by P.R. Vogt and B.E. Tulcholke, pp. 351-378, Geol. Soc. of Am., Boulder, Colo., 1986.

Krawczyk, C.M., T.J. Reston, M.-O. Beslier, and G. Boillot, Evidence for detachment tectonics on the Iberia Abyssal Plain rifted margin, *Proc. Ocean Drill. Program, Sci. Results, 149,* 603-615, 1996.

Latin, D., and N. White, Generating melt during lithospheric extension: Pure shear vs. simple shear, *Geology, 18,* 327-331, 1990.

Louden, K.E., J.-C. Sibuet, and J.-P. Foucher, Variations in heat flow across the Goban Spur and Galicia Bank continental margins, *J. Geophys. Res., 96,* 16131-16150, 1991.

Louden, K.E., J.-C. Sibuet, and F. Harmegnies, Variations in heat flow across the ocean-continent transition in the Iberia abyssal plain, *Earth Planet. Sci. Lett., 151,* 233-254, 1997.

Ludwig, W.J., J.E. Nafe, and C.L. Drake, Seismic refraction, in *The Sea,* edited by A.E. Maxwell, pp. 53-84, Wiley–Interscience, New York, 1970.

Mauffret, A., and L. Montadert, Rift tectonics on the passive continental margin off Galicia (Spain), *Mar. Pet. Geol., 4,* 49-70, 1987.

McKenzie, D.P., Some remarks on the development of sedimentary basins, *Earth Planet. Sci. Lett., 40,* 25-32, 1978.

Muller, M. R., C. J. Robinson, T. A. Minshull, R. S. White, and M. J. Bickle, Thin crust beneath Ocean Drilling Program borehole 735B at the Southwest Indian Ridge?, *Earth Planet. Sci. Lett., 148,* 93-107, 1997.

Ocean Drilling Program (ODP) Leg 173 Shipboard Scientific Party, Drilling reveals transition from continental breakup to early magnetic crust, *Eos Trans. AGU, 79,* 180-181, 1998.

Osler, J.C., and K.E. Louden, Extinct spreading center in the Labrador Sea: Crustal structure from a two-dimensional seismic refraction velocity model, *J. Geophys. Res., 100,* 2261-2278, 1995.

Peddy, C., B. Pinet, D. Masson, R. Scrutton, J.-C. Sibuet, M.R. Warner, J.-P. Lefort, and I.J. Shroeder, Crustal structure of the Goban Spur continental margin, northeast Atlantic, from deep seismic reflection profiling, *J. Geol. Soc. London, 146,* 427-437, 1989.

Pedersen, T., and H. E. Ro, Finite duration extension and decompression melting, *Earth Planet. Sci. Lett., 113,* 15-22, 1992.

Pickup, S.L.B., R.B. Whitmarsh, C.M.R Fowler, and T.J. Reston, Insight into the nature of the ocean-continent transition off West Iberia from a deep multichannel seismic reflection profile, *Geology, 24,* 1079-1082, 1996.

Pinheiro, L.M., R.B. Whitmarsh, and P.R. Miles, The ocean-continent boundary off the western continental margin of Iberia, II, Crustal structure in the Tagus Abyssal Plain, *Geophys. J. Int., 109,* 106-124, 1992.

Pinheiro, L.M., R.C.L. Wilson, R. Pena dos Reis, R.B. Whitmarsh, and A. Ribeiro, The western Iberia margin: A geophysical and geological overview, *Proc. Ocean Drill. Program, Sci. Results 149,* 3-23, 1996.

Reid, I.D., Crustal structure of a nonvolcanic rifted margin east of Newfoundland, *J. Geophys. Res., 99,* 15161-15180, 1994.

Reid, I.D., and C.E. Keen, High seismic velocities associated with reflections from within the lower oceanic crust near the continental margins of eastern Canada, *Earth Planet. Sci. Lett., 99,* 118-126, 1990.

Reston, T.J., The *S* reflector west of Galicia: the seismic signature of a detachment fault, *Geophys. J. Int., 127,* 230-244, 1996.

Sawyer, D.S., et al., *Proceedings of the Ocean Drilling Program, Initial Reports,* vol. 149, Ocean Drill. Program, College Station, Tex., 1994.

Seifert, K. E., C. Cheng-Wen, and D. A. Brunotte, Evidence from Ocean Drilling Program Leg 149 mafic igneous rocks for oceanic crust in the Iberia Abyssal Plain ocean-continent transition zone, *J. Geophys. Res., 102,* 7915-7928, 1997.

Sibuet, J.-C., Formation of nonvolcanic passive margins: A composite model applied to the conjugate Galicia and southeastern Flemish Cap margins, *Geophys. Res. Lett., 19,* 769-772, 1992.

Sibuet, J.-C., V. Louvel, R.B. Whitmarsh, R.S. White, S.J. Horsefield, B. Sichler, P. Leon, and M. Recq, Constraints on rifting processes from refraction and deep-tow magnetic data: The example of the Galicia continental margin (West Iberia), in *Rifted Ocean-Continent Boundaries,* edited by E. Banda, M. Torne, and M. Talwani, pp. 197-218, Kluwer Acad , Norwell, Mass., 1995.

Srivastava, S.P., and W.R. Roest, Nature of thin crust across the Southwest Greenland margin and its bearing on the location of the ocean-continent boundary, in *Rifted Ocean-Continent Boundaries,* edited by E. Banda et al. , pp. 95-120, Kluwer Acad., Norwell, Mass., 1995.

Srivastava, S. P., and J. Verhoef, Evolution of Mesozoic sedimentary basins around the North Central Atlantic: A preliminary plate kinematic solution, in *Basins of the Atlantic Seaboard: Petroleum Geology, Sedimentology and Basin Evolution,* edited by J. Parnell, *Geol. Soc. Special Publ. London, 62,* pp. 397-420, 1992.

Tucholke, B. E., and W.J. Ludwig, Structure and origin of the J anomaly Ridge, western North Atlantic Ocean, *J. Geophys. Res., 87,* 9389-9407, 1982.

White, R.S., D. McKenzie, and K. O'Nions, Oceanic crustal thickness from seismic measurements and rare earth element inversions, *J. Geophys. Res., 97,* 19683-19715, 1992.

Whitmarsh, R.B., and P.R. Miles, Models of the development of the West Iberia rifted continental margin at 40°30′N deduced from surface and deep-tow magnetic anomalies, *J. Geophys. Res., 100,* 3789-3806, 1995.

Whitmarsh, R.B., and D.S. Sawyer, The ocean-continent transition beneath the Iberia Abyssal Plain and continental-rifting to seafloor-spreading processes, in *Proc. Ocean Drill. Program, Sci. Results, 149,* 713-733, 1996.

Whitmarsh, R.B., P.R. Miles, and A. Mauffret, The ocean-continent boundary off the western continental margin of Iberia, I, Crustal structure at 40°30′N, *Geophys. J. Int., 103,* 509-531, 1990.

Whitmarsh, R.B., L.M. Pinheiro, P.R. Miles, M. Recq, and J.-C. Sibuet,

Thin crust at the western Iberia ocean-continent transition and ophiolites, *Tectonics, 12*, 1230-1239, 1993.

Whitmarsh, R.B., R.S. White, S.J. Horsefield, J.-C. Sibuet, M. Recq, and V. Louvel, The ocean-continent boundary off the western continental margin of Iberia: Crustal structure west of Galicia Bank, *J. Geophys. Res., 101*, 28291-28314, 1996.

Whitmarsh, R.B., et al., *Proceedings of the Ocean Drilling Program, Scientific Results*, vol. 173, Ocean Drill. Program, College Station, Tex., 1998.

Winterer, E.L., J. Gee, and J. van Waasbergen, The source area for Lower Cretaceous clastic sediments of the Galicia Bank margin: Geology and tectonic and erosional history, *Proc. Ocean Drill. Program, Sci. Results, 103*, 697-732, 1988.

Zelt, C.A., and D.A. Forsyth, Modeling wide-angle seismic data for crustal structure: Southeastern Grenville Province, *J. Geophys. Res., 99*, 11687-11704, 1994.

Zelt, C.A., and R.B. Smith, Seismic travel-time inversion for 2-D crustal velocity structure, *Geophys. J. Int., 108*, 16-34, 1992.

D. Chian, Geological Survey of Canada (Atlantic), P.O. Box 1006, Dartmouth, Nova Scotia, Canada B2Y 4A2. (chiand@agc.bio.ns.ca)

K.E. Louden, Department of Oceanography, Dalhousie University, Halifax, Nova Scotia, Canada B3H 4J1. (klouden@is.dal.ca)

T.A. Minshull, Bullard Laboratories, Department of Earth Sciences, University of Cambridge, Madingley Road, Cambridge CB3 0EZ, England, U.K. (minshull@esc.cam.ac.uk)

R.B. Whitmarsh, Challenger Division, Southampton Oceanography Centre, Euroopean Way, Southampton SO14 3ZH, England, U.K. (bob.whitmarsh@soc.soton.ac.uk)

(Received April 20, 1998; revised November 6, 1998; accepted December 17, 1998.)